



SIMULATION AND CONTROL OF SOLAR THERMAL POWER PLANT.



By  
MR. Chanachai MAHOM

A Thesis Submitted in Partial Fulfillment of the Requirements

for Master of Engineering (CHEMICAL ENGINEERING)

Department of CHEMICAL ENGINEERING

Graduate School, Silpakorn University

Academic Year 2020

Copyright of Graduate School, Silpakorn University

การจำลองและการควบคุมโรงไฟฟ้าพลังงานความร้อนแสงอาทิตย์



วิทยานิพนธ์นี้เป็นส่วนหนึ่งของการศึกษาตามหลักสูตรวิศวกรรมศาสตรมหาบัณฑิต  
สาขาวิชาวิศวกรรมเคมี แผน ก แบบ ก 2 ระดับปริญญาโทมหาบัณฑิต  
ภาควิชาวิศวกรรมเคมี  
บัณฑิตวิทยาลัย มหาวิทยาลัยศิลปากร  
ปีการศึกษา 2563  
ลิขสิทธิ์ของบัณฑิตวิทยาลัย มหาวิทยาลัยศิลปากร

SIMULATION AND CONTROL OF SOLAR THERMAL POWER PLANT.



By  
MR. Chanachai MAHOM

A Thesis Submitted in Partial Fulfillment of the Requirements  
for Master of Engineering (CHEMICAL ENGINEERING)  
Department of CHEMICAL ENGINEERING  
Graduate School, Silpakorn University  
Academic Year 2020  
Copyright of Graduate School, Silpakorn University

Title                    Simulation and control of solar thermal power plant.  
By                        Chanachai MAHOM  
Field of Study        (CHEMICAL ENGINEERING)  
Advisor                Assistant Professor VEERAYUT LERSBAMRUNGSUK , D.Eng.

---

Graduate School Silpakorn University in Partial Fulfillment of the Requirements  
for the Master of Engineering

.....Dean of graduate school  
(Associate Professor Jurairat Nunthanid, Ph.D.)

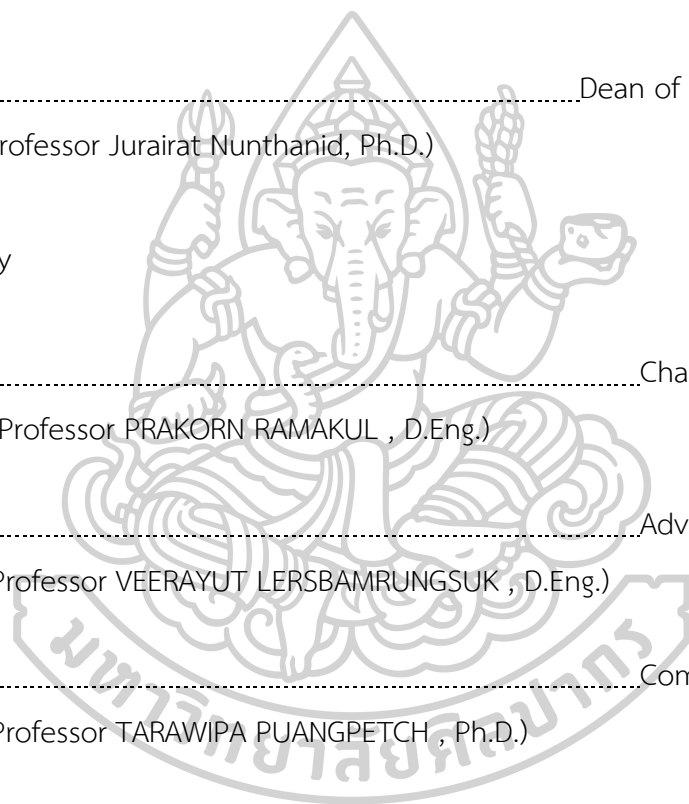
Approved by

.....Chair person  
(Associate Professor PRAKORN RAMAKUL , D.Eng.)

.....Advisor  
(Assistant Professor VEERAYUT LERSBAMRUNGSUK , D.Eng.)

.....Committee  
(Assistant Professor TARAWIPA PUANGPETCH , Ph.D.)

.....External Examiner  
(Professor Thongchai Rohitatisa Srinophakun , Ph.D.)



58404205 : Major (CHEMICAL ENGINEERING)

Keyword : Solar thermal, Dynamic simulation, PI control, MPC control

MR. CHANACHAI MAHOM : SIMULATION AND CONTROL OF SOLAR THERMAL POWER PLANT. THESIS ADVISOR : ASSISTANT PROFESSOR VEERAYUT LERSBAMRUNGSUK, D.Eng.

The demand for energy consumption continuously increases while the availability of fossil energy steadily decreased. Solar energy is one of the main renewable options for power generation. However, unlike other sources of energy that can be manipulated, solar radiation acts as a disturbance that is uncertain and changes seasonal and on a daily base. Hence, control of solar thermal power plants is a challenging task. In this research, dynamic simulations of parabolic trough concentrated solar thermal power plants were performed in both open-loop and closed-loop to investigate the dynamic behavior of the power plant. The process and model used in this paper were adapted from Powell and Edgar. In the open-loop simulation, effects of the flow rate of heat transfer fluid (HTF) to the outlet temperature of the collector and power generation under daily solar radiation were demonstrated. The results showed inherent nonlinearity in the power plant. In the closed-loop simulation, three control configurations including single-loop HTF temperature control, single-loop power control, and dual-loop control (where both HTF temperature and power were controlled) were proposed. PI and MPC controllers were designed for each control configuration. In a closed-loop simulation using PI controller, continuous- and discrete-time PI were implemented. Continuous-time PI was implemented to see the possibility for control of the power plant in the ideal case while discrete-time PI was implemented for the comparison with MPC which was discrete in nature and more realistic. The results showed that continuous-time PI could keep all controlled variables at the setpoint for all control configurations while discrete-time PI and MPC could keep controlled variables at the setpoint for only some cases.

## ACKNOWLEDGEMENTS

The author would like to express his gratitude and appreciation to his advisor, Assistant Professor Dr. Veerayut Lersbamrungsuk for support, stimulating, useful discussions throughout this research.

In addition, the author would like to gratefully acknowledge Associate Professor Dr. Prakorn Ramakul, as the chairman of the committee, Assistant Professor Dr. Tarawipa Puangpetch, and Professor Dr. Thongchai Rohitatisa Srinophakun as the members of the thesis committee for their kind evaluation of work and valuable suggestions that could be beneficially used to improve working behavior.

The support from the Department of Chemical Engineering, Faculty of Engineering and Industrial Technology, Silpakorn University, Thailand has been gratefully acknowledged.

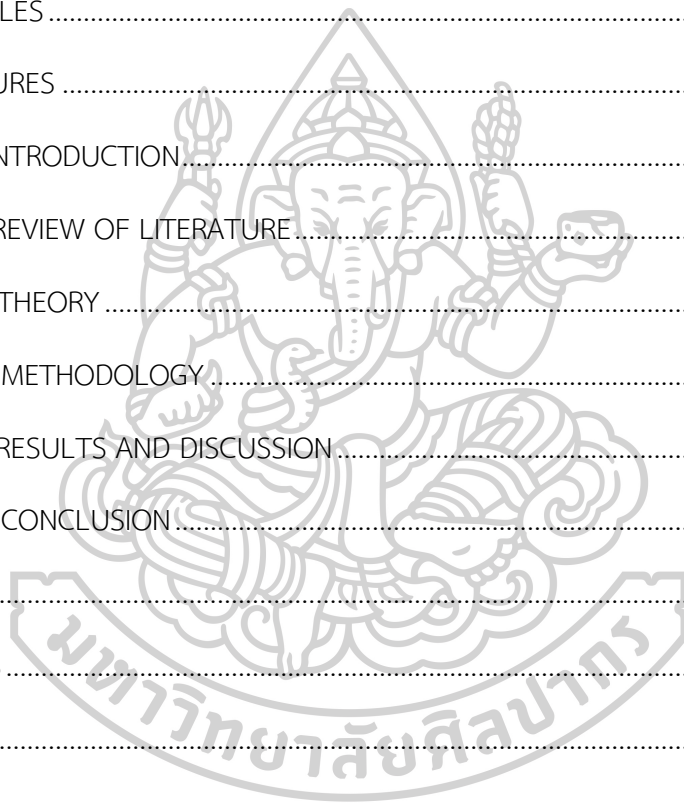
Finally, but most importantly, the author would like to express the highest gratitude to his family and his best friends for their support, encouragement, love, and care.



Chanachai MAHOM

## TABLE OF CONTENTS

	Page
ABSTRACT .....	D
ACKNOWLEDGEMENTS .....	E
TABLE OF CONTENTS .....	F
LIST OF TABLES .....	G
LIST OF FIGURES .....	H
CHAPTER I INTRODUCTION .....	1
CHAPTER II REVIEW OF LITERATURE .....	4
CHAPTER III THEORY .....	10
CHAPTER IV METHODOLOGY .....	15
CHAPTER V RESULTS AND DISCUSSION .....	25
CHAPTER VI CONCLUSION .....	46
APPENDIX A .....	48
REFERENCES .....	52
VITA.....	55



## LIST OF TABLES

	Page
Table 1 IMC-Based PID Controller Settings for $G_c(s)$ [11]. See the text for the rest of this table.....	13
Table 2 Model parameters of the solar thermal power plant. ....	19





## LIST OF FIGURES

	Page
Figure 1 Current and projected world energy use by fuel type. [1].....	1
Figure 2 Type of renewable energy. [2].....	2
Figure 3 Concentration of sunlight using (a) Parabolic trough collector. (b) Linear Fresnel collector. (c) Central receiver system with dish collector. (d) Central receiver system with distributed reflectors. [4].....	3
Figure 4 A solar thermal power plant. [5].....	4
Figure 5 a) One-dimensional steady-state energy balance b) thermal resistance model for a cross-section of an HCE. [6].....	5
Figure 6 Schematic of the two-dimensional heat transfer model. [6].....	6
Figure 7 Schematic diagram of the solar heating system. [9].....	8
Figure 8 Heat transfer and thermal resistance model in a cross-section at the heat collection element (HCE). [10].....	11
Figure 9 Controller action construction using model-based predictive control (MPC) approach. [12].....	14
Figure 10 A parabolic trough solar thermal power plant scheme.....	15
Figure 11 A diagram of the boiler showing the inner-pipe discretization for numerical simulation. [5].....	18
Figure 12 The solar irradiation on the time of day. [14].....	20
Figure 13 Temperature control configuration of parabolic trough solar thermal power plant.....	21
Figure 14 Power control configuration of parabolic trough solar thermal power plant.....	22

Figure 15 The dual-loop control of the solar thermal power plants using PID controllers.....	23
Figure 16 The dual-loop control of the solar thermal power plants using MPC controllers.....	24
Figure 17 Effect of solar radiation during a day on the outlet temperature of the collector (TF) under various flow rates of HTF (mF).....	25
Figure 18 Effect of solar radiation during a day on the power generation of the solar thermal power plant, under various flow rates of HTF (mF). ....	26
Figure 19 Effect of the flow rate of HTF to the outlet temperature of the collector for solar incidence radiation of 450 and 800 W/m <sup>2</sup> .....	26
Figure 20 Effect of the flow rate of HTF to the power generation of the solar thermal power plant for solar incidence radiation of 450 and 800 W/m <sup>2</sup> . ....	27
Figure 21 Closed-loop response of temperature control configuration: (a) the flow rate of HTF, (b) the outlet temperature of the collector, and (c) the power generation of the solar thermal power plant. ....	28
Figure 22 Closed-loop response of power control configuration: (a) the flow rate of HTF, (b) the outlet temperature of the collector, and (c) the power generation of the solar thermal power plant.....	30
Figure 23 Closed-loop response of dual-loop PI control (a) The flow rate of HTF for collectors and cold tank in solar thermal power plants (b) Temperatures for solar thermal power plants (c) Power generation for solar thermal power plants (d) Volume of solar thermal storage tank for solar thermal power plants with solar irradiation is 450 W/m <sup>2</sup> . ....	32
Figure 24 Closed-loop response of dual-loop PI control (a) The flow rate of HTF for collectors and cold tank in solar thermal power plants (b) Temperatures for solar thermal power plants (c) Power generation for solar thermal power plants (d) Volume of solar thermal storage tank for solar thermal power plants with solar irradiation is 800 W/m <sup>2</sup> . ....	34

Figure 25 Closed-loop response of dual-loop PI control (a) The flow rate of HTF for collectors and Boilers in solar thermal power plants (b) Temperatures for solar thermal power plants (c) Power generation for solar thermal power plants (d) Volume of solar thermal storage tank for solar thermal power plants with solar irradiation on the time of day.....	36
Figure 26 Closed-loop response of temperature control configuration with discrete-time PI :(a) the flow rate of HTF, (b) the outlet temperature of the collector, and (c) the power generation of the power plant. ....	38
Figure 27 Closed-loop response of power control configuration with discrete-time PI: (a) the flow rate of HTF, (b) the outlet temperature of the collector, and (c) the power generation of the power plant.....	39
Figure 28 Closed-loop response of temperature control with MPC controller (a) The flow rate of HTF for collectors and Boilers in solar thermal power plants (b) Temperatures for solar thermal power plants (c) Power generation for solar thermal power plants (d) Volume of solar thermal storage tank for solar thermal power plants with solar irradiation is $800 \text{ W/m}^2$ . ....	41
Figure 29 Closed-loop response of power control with MPC controller (a) The flow rate of HTF for collectors and Boilers in solar thermal power plants (b) Temperatures for solar thermal power plants (c) Power generation for solar thermal power plants (d) Volume of solar thermal storage tank for solar thermal power plants with solar irradiation is $800 \text{ W/m}^2$ . ....	43
Figure 30 Closed-loop response of dual-loop control with MPC controller (a) The flow rate of HTF for collectors and Boilers in solar thermal power plants (b) Temperatures for solar thermal power plants (c) Power generation for solar thermal power plants (d) Volume of solar thermal storage tank for solar thermal power plants with solar irradiation is $800 \text{ W/m}^2$ . ....	45
Figure 31 (a) the simulation between the temperature outlet of the collector when the flow rate of HTF changes, (b) the flow rate of HTF changes from $10 \text{ kg/s}$ to $12 \text{ kg/s}$ at $IC = 600 \text{ W/m}^2$ .....	49

Figure 32 (a) the simulation between the power generation when the flow rate of HTF changes, (b) the flow rate of HTF changes from 10 kg/s to 12 kg/s at IC = 600 W/m<sup>2</sup>. ..... 51



## CHAPTER I

### INTRODUCTION

The demand for energy consumption is increasing (Figure 1). While the main source of energy is fossil fuel but its depletion makes the need for new sources of renewable energy.

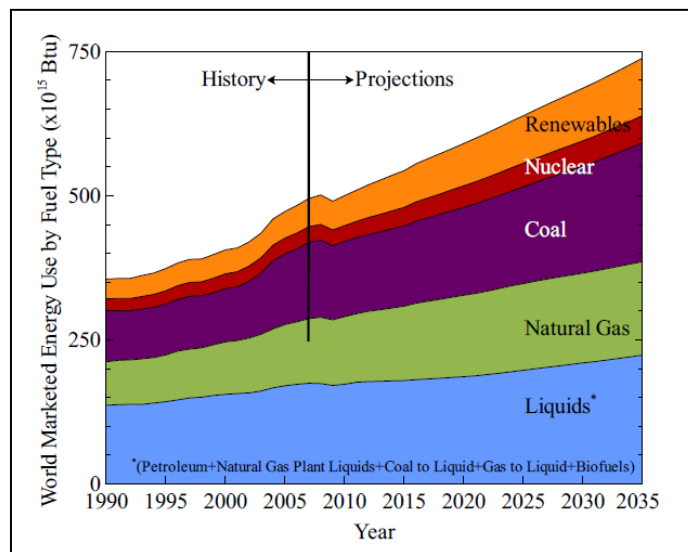


Figure 1 Current and projected world energy use by fuel type. [1]

Renewable energy consists of solar energy, wind energy, tidal energy, biomass energy solar energy geothermal energy, and hydroelectricity as shown in Figure 2. Among these renewable resources, solar energy is one of the main renewable alternatives for the production of electricity. Two technologies are proposed: Photovoltaic (Solar cell) and Solar thermal power plants. Photovoltaic uses semiconductor technology to directly convert sunlight into electricity while Solar thermal uses mirror to concentrate sunlight, which is then used as the heat source for steam generation. Comparison between the two technologies, solar thermal has the advantage in terms of energy storage. Solar thermal stores energy in various heat transfer mediums while photovoltaic stores energy inexpensive battery. This dissertation will focus on solar thermal power plants.



Figure 2 Type of renewable energy. [2]

Power plants with concentrators produced for electricity consist of four technologies: Parabolic Trough Collector (PTC), Linear Fresnel Reflector System (LF), Power Tower or Central Receiver System (CRS), and Dish/Engine system (DE). The characteristics of each solar technology show in Figure 3.

From Figure 3, this dissertation will focus on the parabolic trough collector which is considered as one of the most mature applications of solar energy in this field [3]. Since it reduces the costs, convenient to upscale, and can be set up to use fossil fuel as a supplementary fuel.

A major drawback of solar energy is the uncertainty of the energy source, i.e., sunlight. Solar radiation is not constant throughout the day due to many factors including time, season, weather. This uncertainty can make a variation of the temperature of heat transfer fluid directly affecting the efficiency of the power plant. Furthermore, the sunlight period and variation of electricity demand make the operation of the power plant more complicated. This results in a challenging task to design a control system for a solar thermal power plant. In this research, a solar

thermal power plant will be modeled and simulated. Then control system will be designed to ensure smooth operation of the plant.

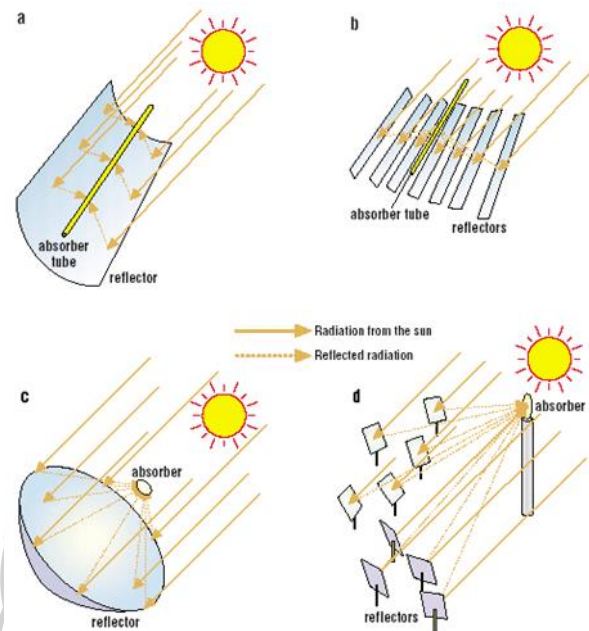


Figure 3 Concentration of sunlight using (a) Parabolic trough collector. (b) Linear Fresnel collector. (c) Central receiver system with dish collector. (d) Central receiver system with distributed reflectors. [4]

### Objective of Research

Simulation and control of solar thermal power plant.

### Scope of research

- 1 Perform the process flow sheet of parabolic trough solar thermal power plants adapted from [5]
- 2 Modeling and analysis of heat transfer of parabolic trough solar thermal power plants adapted from [5]
- 3 Design control system for parabolic trough solar thermal power plants
- 4 The solar radiation incident will be collected from measurement data in Thailand.

## CHAPTER II

### REVIEW OF LITERATURE

#### Reviews on Solar thermal power plant

[5] proposed the dynamic simulation for a thermal storage unit used in a parabolic trough concentrated solar power and design process for a two-tank direct method to generate the model of process (Figure 4). The process focuses on controlling the outlet temperature of the solar collector as a single unit and energy storage to supply in the process if the solar radiation decreases or at the night. This research proposes the process flow sheet, energy and mass balance of solar thermal power plants to use in dynamic simulation and compare between the system with no storage and system have storage. The result of research found that the case with thermal energy storage will have energy using to the night and reduce the supplementary fuel requirement by as much as 43%.

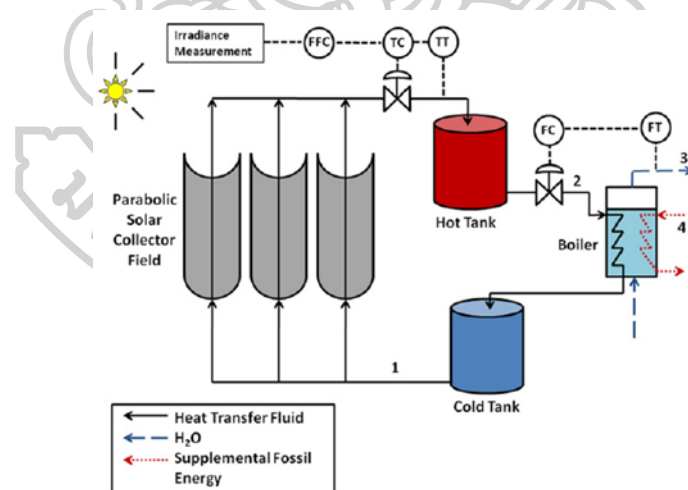


Figure 4 A solar thermal power plant. [5]

[6] proposed heat transfer analysis and modeling of parabolic trough solar receivers. The model determines the performance of a parabolic trough solar collector's linear receiver, also called a heat collector element (HCE) (Figure 5). All heat transfer and thermodynamic equations, optical properties, and parameters used



in the model are discussed. The modeling assumptions and limitations are also discussed, along with recommendations for model improvement. The model was implemented in EES in four different versions (Figure 6). Two versions were developed for conducting HCE design and parameter studies, and two versions were developed for verifying the model and evaluating field test data. While comparing between software model and experimental results, and provided numerous HCE design insights from the design and parameter study.

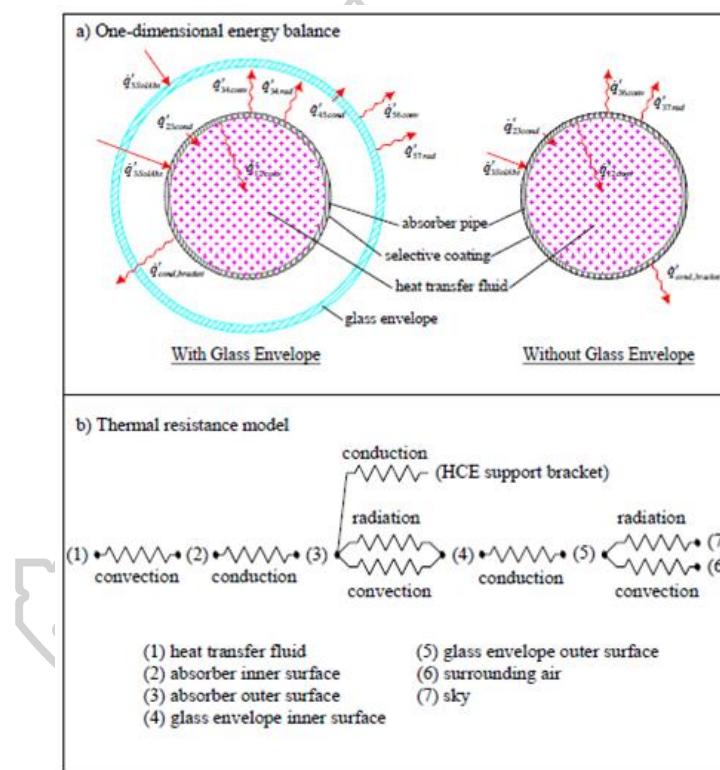


Figure 5 a) One-dimensional steady-state energy balance b) thermal resistance model for a cross-section of an HCE. [6]

The One-dimensional steady-state energy balance equations:

$$\dot{q}'_{Heatloss} = \dot{q}'_{36conv} + \dot{q}'_{37rad} + \dot{q}'_{cond,bracket} \quad (1)$$

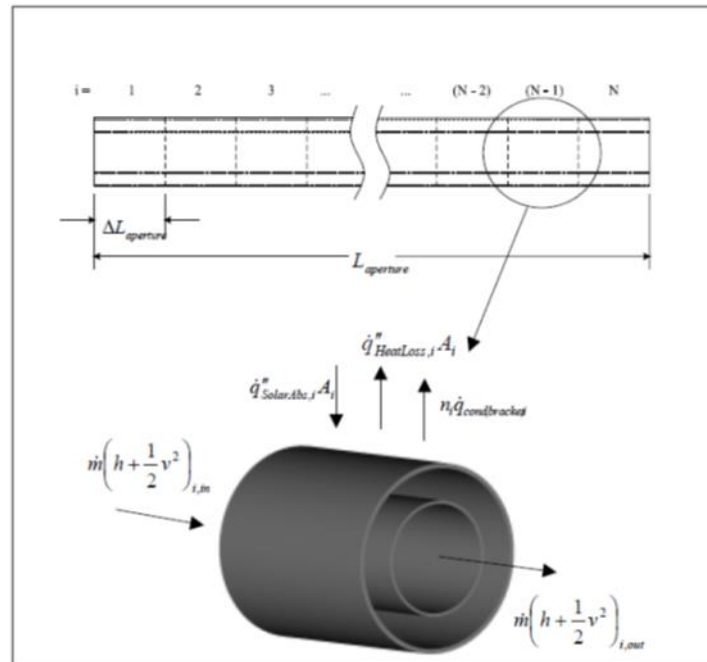


Figure 6 Schematic of the two-dimensional heat transfer model. [6]

The two-dimensional steady-state energy balance:

$$\dot{q}''_{Heatloss} = \dot{q}'_{57rad,i} \Delta L_{aperture} + \dot{q}'_{56conv,i} \Delta L_{aperture} + \dot{q}'_{cond,bracket,total,i} \Delta L_{aperture} \quad (2)$$

[7] studied the thermal performance of parabolic trough solar collectors while the focus for the thermodynamics of a Parabolic Trough Solar Collector (PTC) plays an important role in solar energy and the efficiency of the collectors. This research presents an up-to-date review of the thermal performance of PTC collectors. Various types of mathematical models, simulation and numerical methods, and experimental setups of the Parabolic Trough Solar Collectors are reviewed. These have been studied in terms of heat loss, environmental conditions, and temperature and heat flux. Furthermore, the report cost analysis and economic strategy are used for PTC collectors.

[8] proposed modeling simulation and performance analysis of parabolic trough solar collectors. While numerical studies have been conducted to assess and

improve the performance of parabolic through solar collectors. This review methodologically holds colossal knowledge of current and past studies to assess the optical and thermal performances of parabolic trough solar collectors, modeling approaches, and the potential improvements proposed on behalf of the parabolic trough solar collector design. The optical modeling approaches are identified to be analytical and ray-tracing. The review of thermal modeling approaches presents the steady and transient heat transfer analyses of single and two-phase flows. Also, the computational fluid dynamics models are used to analyze the physics of parabolic through solar collectors.

[9] proposed applicability analysis of the solar heating system with parabolic trough solar collectors in different regions of China, which parabolic trough solar collectors (PTCs) were operated with the absorption heat pumps (AHP) and oil/water heat exchanger (OWHE) at medium and low operating temperature respectively (Figure 7). The heat transfer model for PTCs was constructed with a lumped parameter method and validated by experimental results. This research showed the result of operating with low direct normal irradiance (DNI) and high DNI case. At low direct normal irradiance (DNI), the operation of the PTC+AHP/OWHE system was not cost-effective and on cloudy days (high DNI) the operation of the PTC+OWHE system was better than that of the PTC+AHP system as the latter needed more preheating energy before the system operation.

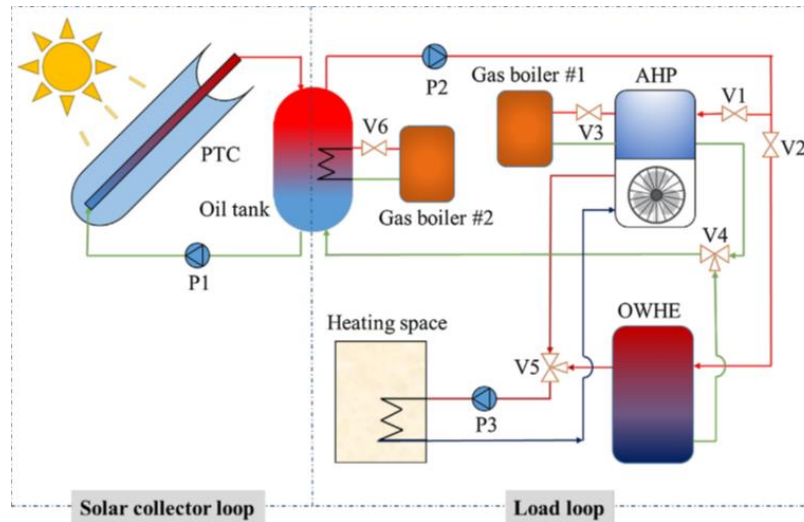


Figure 7 Schematic diagram of the solar heating system. [9]

[10] proposed a detailed one-dimensional numerical heat transfer analysis of a PTC is performed. The receiver and envelope were divided into several segments and mass and energy balance were applied in each segment. Improvements either in the heat transfer correlations or radiative heat transfer analysis are presented as well. The partial differential equations were discretized and the nonlinear algebraic equations were solved simultaneously. Also, validate the numerical results, the model was compared with experimental data obtained from Sandia National Laboratory (SNL) and other one-dimensional heat transfer models. The result has been compared between experimental data and other models. The energy balance following:

Heat transfer from the absorber to heat transfer fluid:

$$A_{i,a}\rho_f C_{p,f} \frac{\partial T_f}{\partial t} = -\dot{m}_f \frac{\partial}{\partial z} \left( C_{p,i} T_f + \frac{v_f^2}{2} \right) + \dot{Q}'_{a-f,conv} \quad (3)$$

Heat transfer from the absorber to glass envelope:

$$A_a \rho_a C_{p,a} \frac{\partial T_a}{\partial t} = A_a \frac{\partial}{\partial z} \left( k_a \frac{\partial T_a}{\partial z} \right) + \dot{Q}'_{a-abs} - \dot{Q}'_{a-f,conv} - \dot{Q}'_{a-e,conv} - \dot{Q}'_{a-e,rad} - \dot{Q}'_{cond,bracket} \quad (4)$$

Heat transfer from glass envelope to the ambient:

$$A_e \rho_e C_{p,e} \frac{\partial T_e}{\partial t} = A_e \frac{\partial}{\partial z} \left( k_e \frac{\partial T_e}{\partial z} \right) + \dot{Q}'_{e-abs} + \dot{Q}'_{a-e,conv} + \dot{Q}'_{a-e,rad} - \dot{Q}'_{e-sa,conv} - \dot{Q}'_{e-s,rad} \quad (5)$$



## CHAPTER III

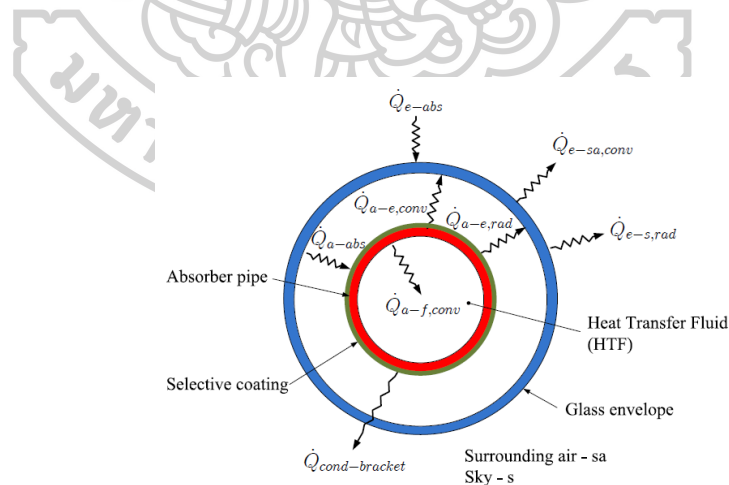
### THEORY

#### 3.1. A parabolic trough solar thermal power plant

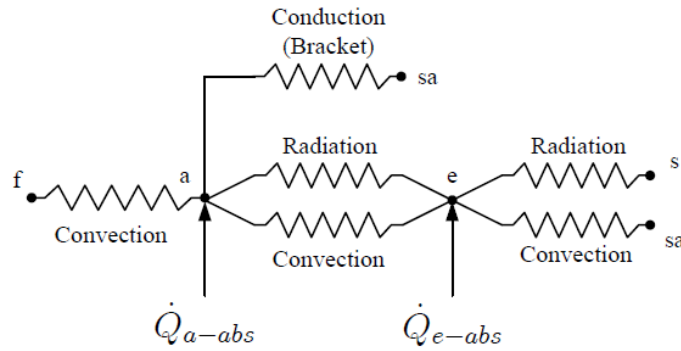
The current parabolic trough power plant is the most fully developed technology for solar thermal power generation. A parabolic trough solar collector (PTC) receives energy radiating from the sun and converts it into useful heat energy in heat-transfer fluid (HTF) circulating through a solar field. PTC synthetic oils are commonly used as HTFs.

These accumulator heat transfer analyzes are important for the calculation of heat loss. The heat collection element (HCE) consists of an absorber surrounded by a glass envelope. The absorber is usually a stainless-steel tube with a selective absorber surface that provides the desired optical and radiant properties.

The heat transfer model is based on the energy balance between the heat transfer fluid and its surrounding. Figure 8 shows the cross-sectional heat transfer at the solar collector and the heat resistance model used in the analysis of the heat transfer.



(a) Heat transfer



(b) Thermal circuit

Figure 8 Heat transfer and thermal resistance model in a cross-section at the heat collection element (HCE). [10]

The solar energy reflected by the mirrors is absorbed by the glass envelope  $\dot{Q}_{e-abs}$  and the absorber surface  $\dot{Q}_{a-abs}$ . A part of the energy absorbed in the absorber is transferred to the HTF by forced convection  $\dot{Q}_{a-f,conv}$ , the remaining energy is transferred back to the glass envelope by radiation  $\dot{Q}_{a-e,rad}$  and natural convection  $\dot{Q}_{a-e,conv}$  and lost through the support brackets by conduction  $\dot{Q}_{cond,bracket}$  as well. The heat loss coming from the absorber (radiation and natural convection) passes through the glass envelope by conduction and along with the energy absorbed by the glass, the envelope is lost to the environment by convection  $\dot{Q}_{e-sa,conv}$  and to the sky by radiation  $\dot{Q}_{e-s,rad}$ .

The heat collection element (HCE) divide into three sections is Heat Transfer from Absorber to Heat Transfer Fluid, Heat Transfer from Absorber to Glass Envelope, and Radiation Heat Transfer from Receiver to Envelope.

Heat Transfer from Absorber to Heat Transfer Fluid the following partial differential equation (PDE) is obtained:

$$A_{a,i}\rho_f C_{p,f} \frac{\partial T_f}{\partial t} = -\dot{m}_f \frac{\partial}{\partial z} \left( C_{p,f} T_f + \frac{V_f^2}{2} \right) + \dot{Q}'_{a-f,conv} \quad (6)$$

$$V_f = \frac{\dot{m}_f}{A_{a,i}\rho_f} \quad (7)$$

where  $A_{a,i}$  is the internal cross-sectional area of the absorber.

Heat Transfer from Absorber to Glass Envelope the following partial differential equation (PDE) is obtained:

$$A_a \rho_a C_{p,a} \frac{\partial T_a}{\partial t} = A_a \frac{\partial}{\partial z} \left( k_a \frac{\partial T_a}{\partial z} \right) + \dot{Q}'_{a-abs} - \dot{Q}'_{a-f,conv} - \dot{Q}'_{a-e,conv} - \dot{Q}'_{a-e,rad} - \dot{Q}'_{cond,bracket} \quad (8)$$

Radiation Heat Transfer (Sky and Collector Surface) the following partial differential equation (PDE) is obtained:

$$A_e \rho_e C_{p,e} \frac{\partial T_e}{\partial t} = A_e \frac{\partial}{\partial z} \left( k_e \frac{\partial T_e}{\partial z} \right) + \dot{Q}'_{e-abs} + \dot{Q}'_{a-e,conv} + \dot{Q}'_{a-e,rad} - \dot{Q}'_{e-sa,conv} - \dot{Q}'_{e-s,rad} \quad (9)$$

### 3.2 PID control

#### 3.2.1 First-Order-plus-Time-Delay (FOPTD)

Model Consider the standard FOPTD model.

$$\tilde{G}(s) = \frac{K e^{-\theta s}}{\tau s + 1} \quad (10)$$

Substituting Equation 6 into  $G_c = \frac{1}{\tilde{G}(\tau_c + \theta)s}$  and rearranging gives a PI controller,

$G_c = K_c(1 + 1/\tau_I s)$  with the following controller settings:

$$K_c = \frac{1}{K} \frac{\tau}{\theta + \tau_c} \quad (11)$$

#### 3.2.2 IMC Tuning Relations

The IMC method can be used to derive PID controller settings for a variety of transfer function models.



Table 1 IMC-Based PID Controller Settings for  $G_c(s)$  [11]. See the text for the rest of this table.

Case	Model	$K_c K$	$\tau_I$	$\tau_D$
A	$\frac{K}{\tau s + 1}$	$\frac{\tau}{\tau_c}$	$\tau$	—
B	$\frac{K}{(\tau_1 s + 1)(\tau_2 s + 1)}$	$\frac{\tau_1 + \tau_2}{\tau_c}$	$\tau_1 + \tau_2$	$\frac{\tau_1 \tau_2}{\tau_1 + \tau_2}$
C	$\frac{K}{\tau^2 s^2 + 2\zeta \tau s + 1}$	$\frac{2\zeta \tau}{\tau_c}$	$2\zeta \tau$	$\frac{\tau}{2\zeta}$
D	$\frac{K(-\beta s + 1)}{\tau^2 s^2 + 2\zeta \tau s + 1}$ , $\beta > 0$	$\frac{2\zeta \tau}{\tau_c + \beta}$	$2\zeta \tau$	$\frac{\tau}{2\zeta}$
E	$\frac{K}{s}$	$\frac{2}{\tau_c}$	$2\tau_c$	—
F	$\frac{K}{s(\tau s + 1)}$	$\frac{2\tau_c + \tau}{\tau_c^2}$	$2\tau_c + \tau$	$\frac{2\tau_c \tau}{2\tau_c + \tau}$
G	$\frac{K e^{-\theta s}}{\tau s + 1}$	$\frac{\tau}{\tau_c + \theta}$	$\tau$	—
H	$\frac{K e^{-\theta s}}{\tau s + 1}$	$\frac{\tau + \frac{\theta}{2}}{\tau_c + \frac{\theta}{2}}$	$\tau + \frac{\theta}{2}$	$\frac{\tau \theta}{2\tau + \theta}$

### 3.3 MPC control

The model-based predictive control (MPC) methodology is also referred to as the moving horizon control or the receding horizon control. The MPC is constructed using control and optimization tools. The objective of this write-up is to introduce the reader to the linear MPC which refers to the family of MPC schemes in which linear models of the controlled objects are used in the control law synthesis. In the MPC approach, the current control action is computed online rather than using a pre-computed, off-line, control law. A model predictive controller uses, at each sampling instant, the plant's current input and output measurements, the plant's current state, and the plant's model to calculate, over a finite horizon, a future control sequence that optimizes a given performance index and satisfies constraints on the control action and use the first control in the sequence as the plant's input. The MPC strategy is illustrated in Figure 9, where  $N_p$  is the prediction horizon,  $u(t+k|t)$

is the predicted control action at  $t + k$  given  $u(t)$ . Similarly,  $y(t + k|t)$  is the predicted output at  $t + k$  given  $y(t)$ .

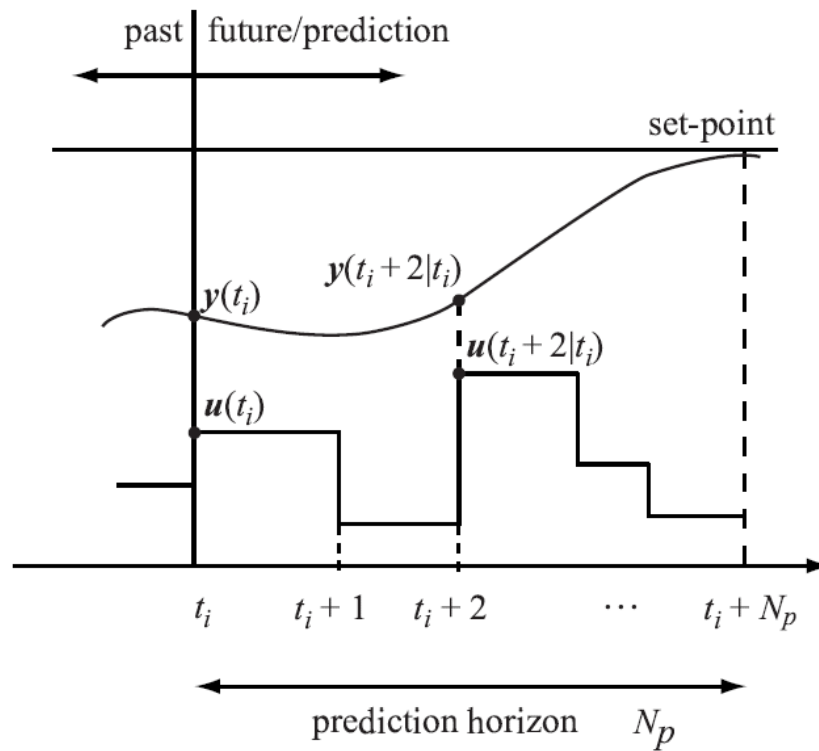


Figure 9 Controller action construction using model-based predictive control (MPC) approach. [12]



## CHAPTER IV

### METHODOLOGY

#### 4.1 Mathematical Model of Solar Thermal Power Plant

The solar thermal power plant consists of two major sections including solar collector and power block as shown in Figure 10. The solar collector considered here is the parabolic trough that uses mirrors to concentrate direct solar radiation to the absorber pipe in which heat is absorbed by the heat transfer fluid (HTF). The hot HTF is stored in the hot storage tank and delivered as the heat source to the boiler for steam generation. In case the heat from HTF is not enough, the external heat source is supplied to the boiler as needed. The used HTF is stored in the cold storage tank and delivered to absorb heat from sunlight. Steam generated in the boiler is transferred to other units such as the turbine for electrical generation.

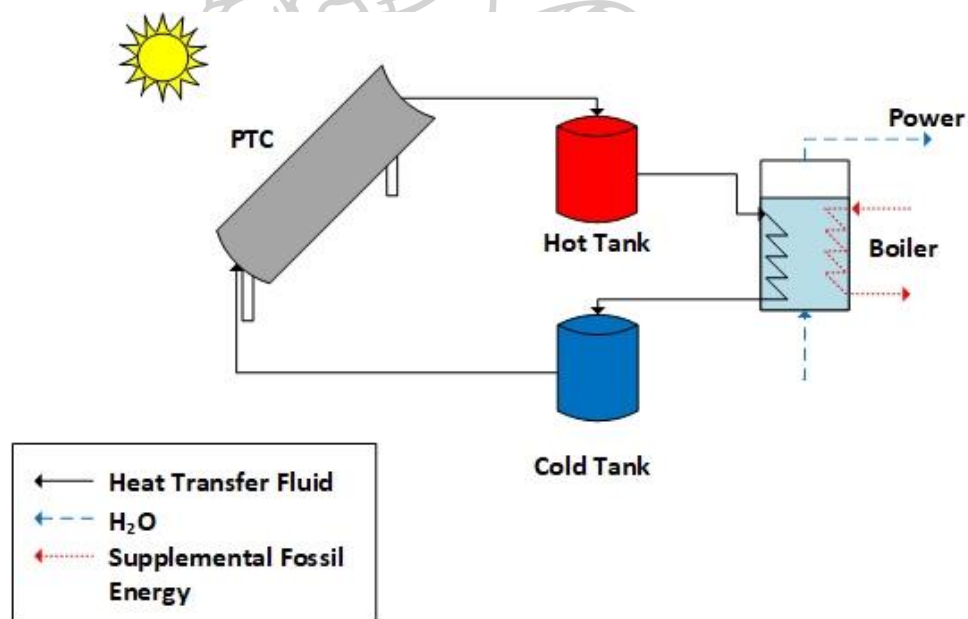


Figure 10 A parabolic trough solar thermal power plant scheme.

##### 4.1.1 Dynamic model of the Parabolic Trough Solar Collector

The dynamic model of parabolic trough solar collector can be derived by performing energy balance. Some assumptions made include neglecting radial

temperature gradients and conductive heat transfer yields, that convection is the dominant mode of heat transfer from the absorber pipe to the HTF. The convection between absorber pipe and glass envelope is neglected due to the vacuum between the two surfaces and neglecting heat loss to the bracket. This leaves radiation as the dominant mode of heat transfer between these two surfaces. The radiative term includes a view factor between two concentric cylinders. As given by [5]. Variations of the emissivity of the absorber pipe and the glass envelope with temperature are neglected.

Due to spatial variation of the temperature, the parabolic trough solar collector can be modeled as partial differential equations (PDEs) as shown in equations 12-14,

Energy balance between heat transfer fluid and absorber pipe:

$$\frac{dT_f}{dt} = \frac{-\dot{m}_f}{A_{a,i}\rho_f} \frac{dT_f}{dx} + \frac{h_p P_{a,i}}{A_{a,i}\rho_f C_f} (T_f - T_a) \quad (12)$$

Energy balance between absorber pipe and glass envelope:

$$\frac{dT_a}{dt} = -\frac{h_p P_{a,i}}{A_a \rho_a C_a} (T_f - T_a) - \frac{\sigma}{\frac{1}{\varepsilon_a} + \frac{1-\varepsilon_a}{\varepsilon_e}} \frac{P_{a,o}(T_a^4 - T_e^4)}{A_a \rho_a C_a} + \frac{I_c \eta_{optical} \omega}{A_a \rho_a C_a} \quad (13)$$

Energy balance between glass envelope and surrounding:

$$\frac{dT_e}{dt} = \frac{\sigma}{\frac{1}{\varepsilon_a} + \frac{1-\varepsilon_a}{\varepsilon_e}} \frac{P_{a,i}(T_a^4 - T_e^4)}{A_e \rho_e C_e} - \frac{\sigma \varepsilon_e P_{e,o}(T_e^4 - T_{SKY}^4)}{A_e \rho_e C_e} - \frac{h_{AIR} P_{e,o}}{A_e \rho_e C_e} (T_e - T_{AIR}) \quad (14)$$

#### 4.1.2 Power Block

##### 4.1.2.1 The thermal energy storage tanks

The thermal energy storage tanks can be modeled using mass and energy balance around tanks. Assumptions of the system are lump model and no heat transfer occurs from the top or bottom of either tank. The system recommends maximum volume of the tank is 120 m<sup>3</sup>.

The mass balance of the thermal energy storage tanks:

$$\frac{dV}{dt} = \frac{\dot{m}_{in} - \dot{m}_{out}}{\rho_f} \quad (15)$$

The energy balance of the thermal energy storage tanks:

$$\frac{dT}{dt} = \frac{T_{in}\dot{m}_{in} - T_{out}\dot{m}_{out}}{V\rho_f} - \frac{UA_{tank}}{C_f\rho_f V} (T - T_{AIR}) - \frac{T}{V} \left( \frac{\dot{m}_{in} - \dot{m}_{out}}{\rho_f} \right) \quad (16)$$

In the initialization of the system, assuming that the cold tank is full of HTF at a low temperature and the hot tank is at its lower-limit volume at some elevated temperature. Furthermore, to prevent overflow and underflow of the tank, some logics are made as follows,

The logic of the tank following in models

$$\text{if } V_{Tank} = V_{high} \text{ and } \dot{m}_{in,controlled} > \dot{m}_{out,controlled} \quad (17)$$

$$\text{then } \dot{m}_{in} = \dot{m}_{out} = \dot{m}_{out,control} \quad (18)$$

$$\text{if } V_{Tank} = V_{low} \text{ and } \dot{m}_{in,controlled} < \dot{m}_{out,controlled} \quad (19)$$

$$\text{then } \dot{m}_{in} = \dot{m}_{out} = \dot{m}_{in,control} \quad (20)$$

#### 4.1.2.2 The boiler

In the boiler, the HTF inside the coil exchanges is used to heat saturated liquid water to generate saturated steam as shown in Figure 11. The assumption is that the temperature on the waterside is constant due to water vaporization while the temperature of HTF varies with time and distance along with the coil. The boiler can be modeled as the equations 21-23,

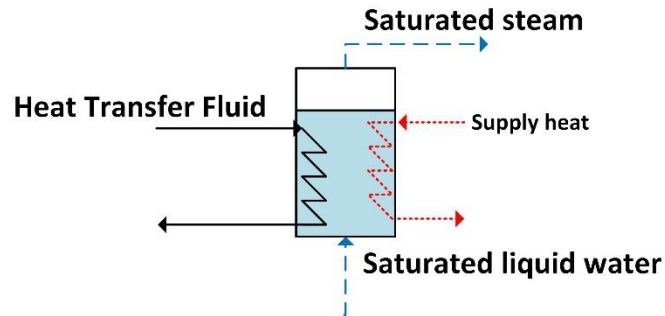


Figure 11 A diagram of the boiler showing the inner-pipe discretization for numerical simulation. [5]

energy balance on heat transfer fluid,

$$\frac{dT_{fB}}{dt} = \frac{\dot{m}_f}{\rho_f A_{p,i}} \frac{dT_{fB}}{dz} + \frac{h_p P_{p,i}}{\rho_f C_f A_{p,i}} (T_B - T_{fB}) \quad (21)$$

steady-state energy balance of saturated steam flow rate on the boiler:

$$\dot{m}_{steam} = \frac{\dot{m}_f C_f}{H_{fg}} (T_{fB,in} - T_{fB,out}) \quad (22)$$

Power generation calculated from.

$$Power = \dot{m}_{steam} H_{fg} \quad (23)$$

#### 4.1.3 Parameters and Some Correlations

The convective heat transfer coefficient can be calculated from the Dittus-Boelter correlation for the Nusselt number for turbulent flow in a circular pipe. [13]

$$h_p = \frac{k Nu_D}{D} \quad (24)$$

$$Nu_D = 0.023 Re_D^{0.8} Pr^{0.4} \quad (25)$$

$$Pr = \frac{\mu}{\rho \alpha}, \quad \alpha = \frac{k}{\rho C_p} \quad (26)$$

The Reynolds number can be calculated in mass flow rate form [10].

$$Re_D = \frac{\dot{m}}{30\pi r \mu} \quad (27)$$

$$\left[ \begin{array}{l} Re_D \geq 10,000 \\ 0.7 \geq Pr \geq 160 \\ \frac{L}{D} \geq 10 \end{array} \right] \quad (28)$$

Table 2 Model parameters of the solar thermal power plant.

Parameter	Value	Parameter	Value
$A_a$ (m <sup>2</sup> )	$8.6 \times 10^{-4}$	$C_f$ (J/kg K)	2300
$A_{a,i}$ (m <sup>2</sup> )	$1.9 \times 10^{-3}$	$C_a$ (J/kg K)	460
$A_e$ (m <sup>2</sup> )	$2.8 \times 10^{-3}$	$C_e$ (J/kg K)	860
$A_{p,i}$ (m <sup>2</sup> )	$2.8 \times 10^{-3}$	$\rho_f$ (kg/m <sup>3</sup> )	1794.1
$r_{a,i}$ (m)	0.025	$\rho_a$ (kg/m <sup>3</sup> )	7850
$r_{a,o}$ (m)	0.03	$\rho_e$ (kg/m <sup>3</sup> )	2400
$r_{e,i}$ (m)	0.03	$\rho_{AIR}$ (kg/m <sup>3</sup> )	1.14152
$r_{e,o}$ (m)	0.0421	$\mu_f$ (kg/m s)	0.0021
$r_{p,i}$ (m)	0.03	$\mu_{AIR}$ (kg/m s)	2.0014
$P_{a,i}$ (m)	0.16	$k_f$ (W/m K)	0.537
$P_{a,o}$ (m)	0.19	$k_{AIR}$ (W/m K)	2699.8
$P_{e,o}$ (m)	0.265	$\sigma$ (W/m <sup>2</sup> K <sup>4</sup> )	$5.67 \times 10^{-8}$
$P_{p,i}$ (m)	0.19	$\epsilon_a$	0.18

$T_B(C^\circ)$	250	$\varepsilon_e$	0.9
<b>Parameter</b>	<b>Value</b>	<b>Parameter</b>	<b>Value</b>
$H_{fg}(J/kg)$	1715	W (m)	2.5
L(m)	200		

#### 4.1.4 Solar Irradiance

In the simulation of the solar thermal power plant, information on solar radiation is needed. In this paper, the amount of radiation incident on the reflector surface (IC) of a day in Thailand [14], A as shown in Figure 12 was used. The sunlight is active during 07.00-18.00 of a day in May 2018.

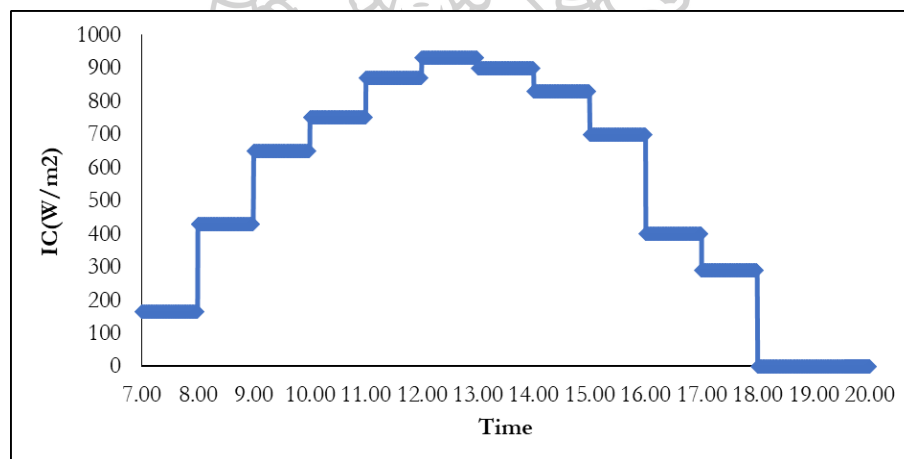


Figure 12 The solar irradiation on the time of day. [14]

#### 4.2 Control Configuration of The Solar Thermal Power Plant

In the closed-loop design of the plant, this work firstly considered a simple single-loop control configuration. By excluding hot and cold storage tanks that resulting in a single HTF flow rate as a manipulated variable. Hence, only one controlled variable is possible. After that, a dual-loop configuration is proposed. In this configuration, hot and cold storage tanks are introduced, and hence, there are two manipulated variables, i.e., HTF flow rate in the charging line (or HTF line passing



the collector) and HTF flow rate in the discharging line (or HTF line passing the boiler).

#### 4.2.1 Closed-loop simulation with single loop control

In control of the Solar Thermal power plant, the manipulated variable of the system is the flow rate of HTF while two possible controlled variables are the outlet temperature of the collector and power generation. Hence, two control configurations including temperature control and power control configurations are proposed. PID control is chosen as the controller for simplicity. The tuning parameters of the process can be found using IMC tuning as shown in the appendix A. [11]

##### 4.2.1.1 Temperature Control Configuration

In the temperature control configuration, as shown in Figure 13, the outlet temperature of the collector is kept at 390 °C by manipulating the flow rate of HTF.

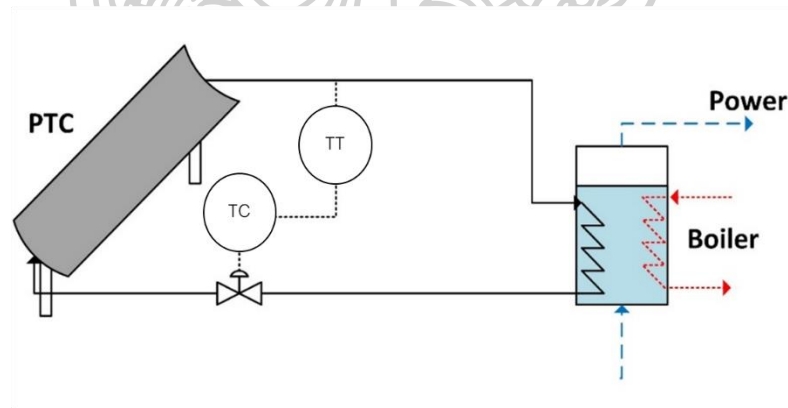


Figure 13 Temperature control configuration of parabolic trough solar thermal power plant.

##### 4.2.1.2 Power Control Configuration

In power control configuration as shown in Figure 14, the power generation targeting is set at 1 MW by manipulating the flow rate of HTF.

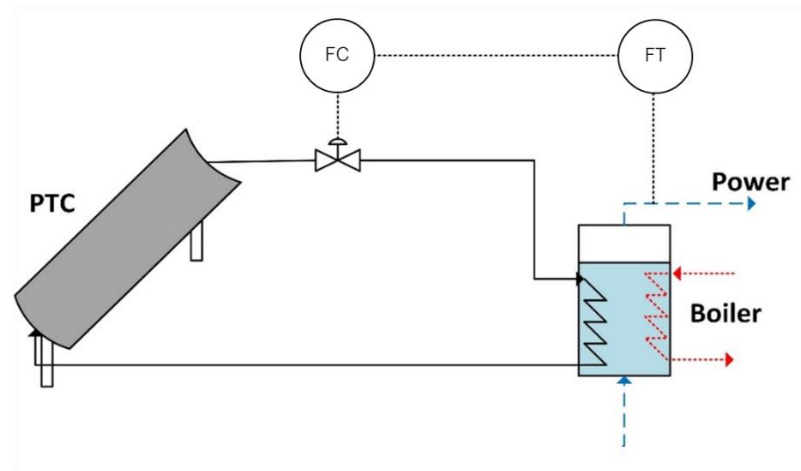


Figure 14 Power control configuration of parabolic trough solar thermal power plant.

#### 4.2.2 Closed-loop simulation with dual-loop control

##### 4.2.2.1 Dual loop control using PID controllers

To improve the performance of the plant by controlling both HTF outlet temperature and power generation, a dual-loop control of the plant is proposed. To have two manipulated variables two tanks including hot and cold tanks are introduced. The configuration is shown in Figure 15.

The manipulated variables of the system are the flow rate of HTF out of the collector (charging line) and the flow rate of HTF out of the hot storage tank (discharging line) while two controlled variables are the outlet temperature of the collector and power generation. The outlet temperature of the collector is kept at 390 °C and the power generation kept at 1 MW. PID controllers are for both loops and tuning parameters can be found using IMC tuning. [11]. Some logics (equations 17-20) are also introduced to prevent overflow and underflow of the tanks.

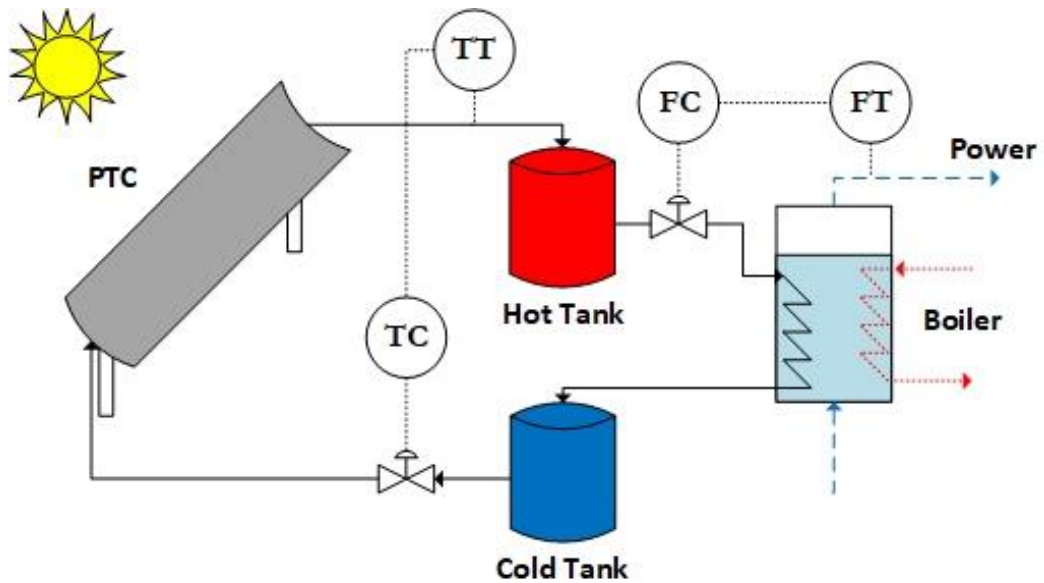


Figure 15 The dual-loop control of the solar thermal power plants using PID controllers.

#### 4.2.2.2 Dual loop control using MPC controllers

To ensure the performance and handling of the interaction of the plant, a multivariable controller, namely, model predictive controller (MPC) is designed and implemented with the help of the MPC toolbox. MPC controller is firstly designed using MPC Designer, then is exported and used in the closed-loop simulation of the power plant. Furthermore, as plant constraints can be included in the MPC, the overflow and underflow conditions of the hot and cold storage tanks can be directly included in the MPC without the need for the introduction of the logic equations 17-20.

Controlled variables are the HTF outlet temperature kept at 390 °C and power generation kept at 1 MW while manipulated variables are HTF flow rate in the charging and discharging lines. Tuning parameters of MPC can be found by adjusting the prediction horizon and control horizon until satisfied performance can be expected.

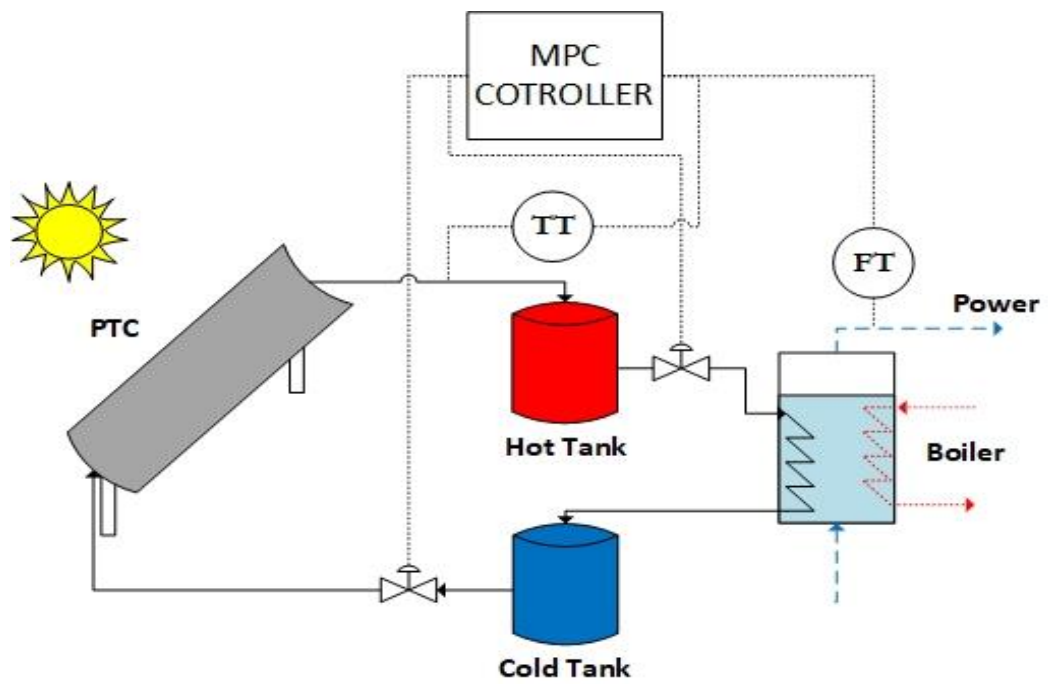


Figure 16 The dual-loop control of the solar thermal power plants using MPC controllers.



## CHAPTER V

### RESULTS AND DISCUSSION

#### 5.1 Open-Loop Simulation

Effects of solar radiation during a day on the outlet temperature of the collector and the power generation of the solar thermal power plant under various flow rates of HTF were shown in Figure 17 and Figure 18. The graph seemed to have the same trend of the solar radiation of a day. The peaks of the temperature and power generation were at around the midday time where the solar radiation was highest. For the effect of the flow rate of HTF, the lower the flow rate of HTF, the higher the outlet temperature was due to more contact time to absorb energy from sunlight. However, for the power generation of the plant, the effect was in contrast because of less amount of HTF for heating in the boiler.

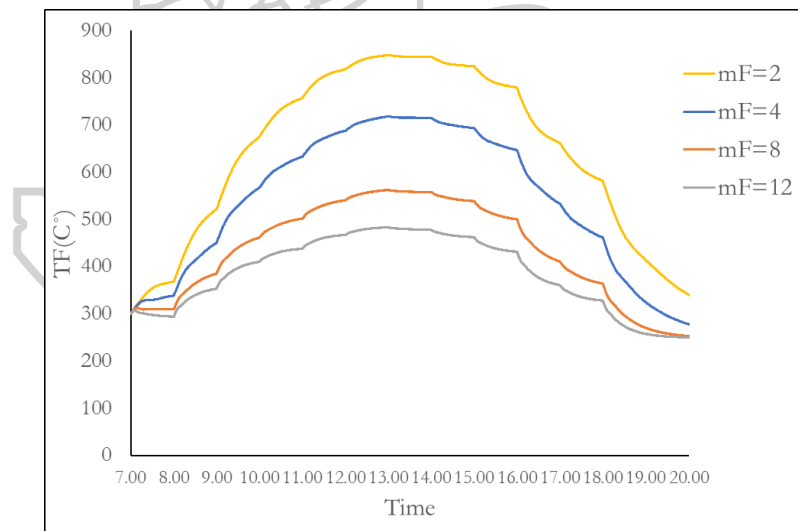


Figure 17 Effect of solar radiation during a day on the outlet temperature of the collector (TF) under various flow rates of HTF (mF).

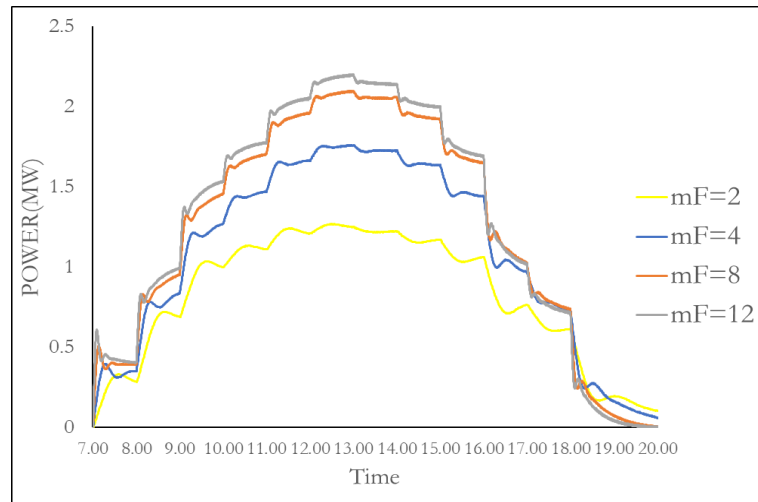


Figure 18 Effect of solar radiation during a day on the power generation of the solar thermal power plant, under various flow rates of HTF (mF).

The effect of the flow rate of HTF on the outlet temperature of the collector and the power generation for solar incidence radiation of 450 and 800  $W/m^2$  was shown in Figures 19 and 20. As the flow rate of HTF increased, the outlet temperature of the collector decreased while the power generation increased. The effects were stronger in the range of low flow rate and this was due to the inherited nonlinearity of the plant. Control. This nonlinearity could affect the control performance of the plant.

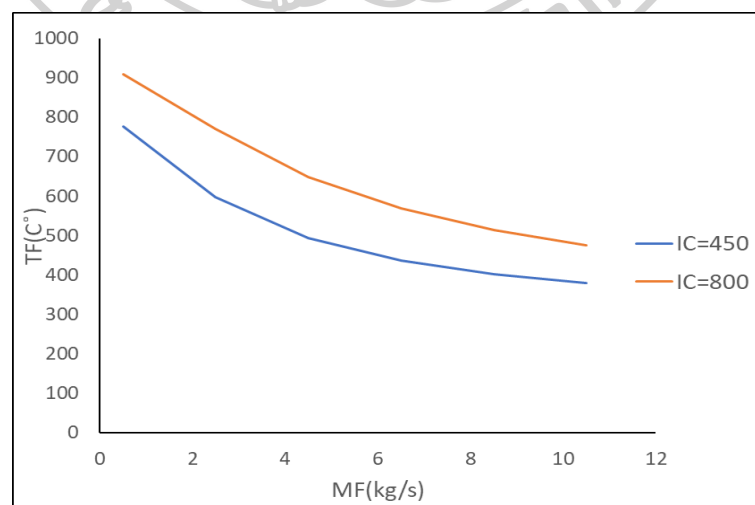


Figure 19 Effect of the flow rate of HTF to the outlet temperature of the collector for solar incidence radiation of 450 and 800  $W/m^2$ .

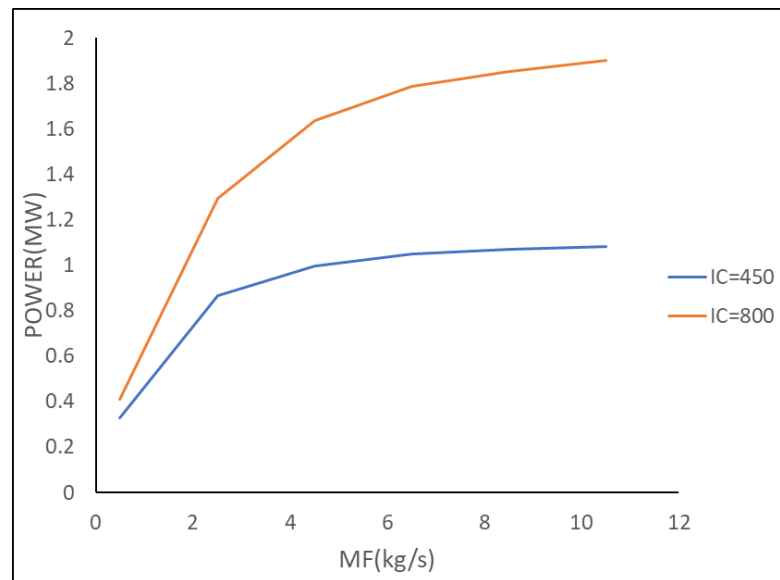


Figure 20 Effect of the flow rate of HTF to the power generation of the solar thermal power plant for solar incidence radiation of 450 and 800  $\text{W/m}^2$ .

## 5.2 Closed-loop simulation with continuous-time PI.

### 5.2.1 Single loop control with temperature control configuration using continuous-time PI.

In temperature control configuration, the PI control system was designed to keep the collector outlet temperature at  $390\text{ }^\circ\text{C}$  by manipulating the flow rate of HTF. The boiler was assumed to be operated at a constant temperature of  $250\text{ }^\circ\text{C}$ . The closed-loop response of the temperature control configuration is shown in Figure 21.

Figure 21b showed during the time 07.00-08.00, the temperature could not reach the target  $390\text{ }^\circ\text{C}$  because there was not enough solar energy. After the time 08.00, the temperature could reach the target and stay there during a day until 18.00 where the sunlight was over, the temperature dropped below the target. Figure 21a showed the manipulation of the flow rate of HTF while Figure 21c showed the power generation which was quite varied.

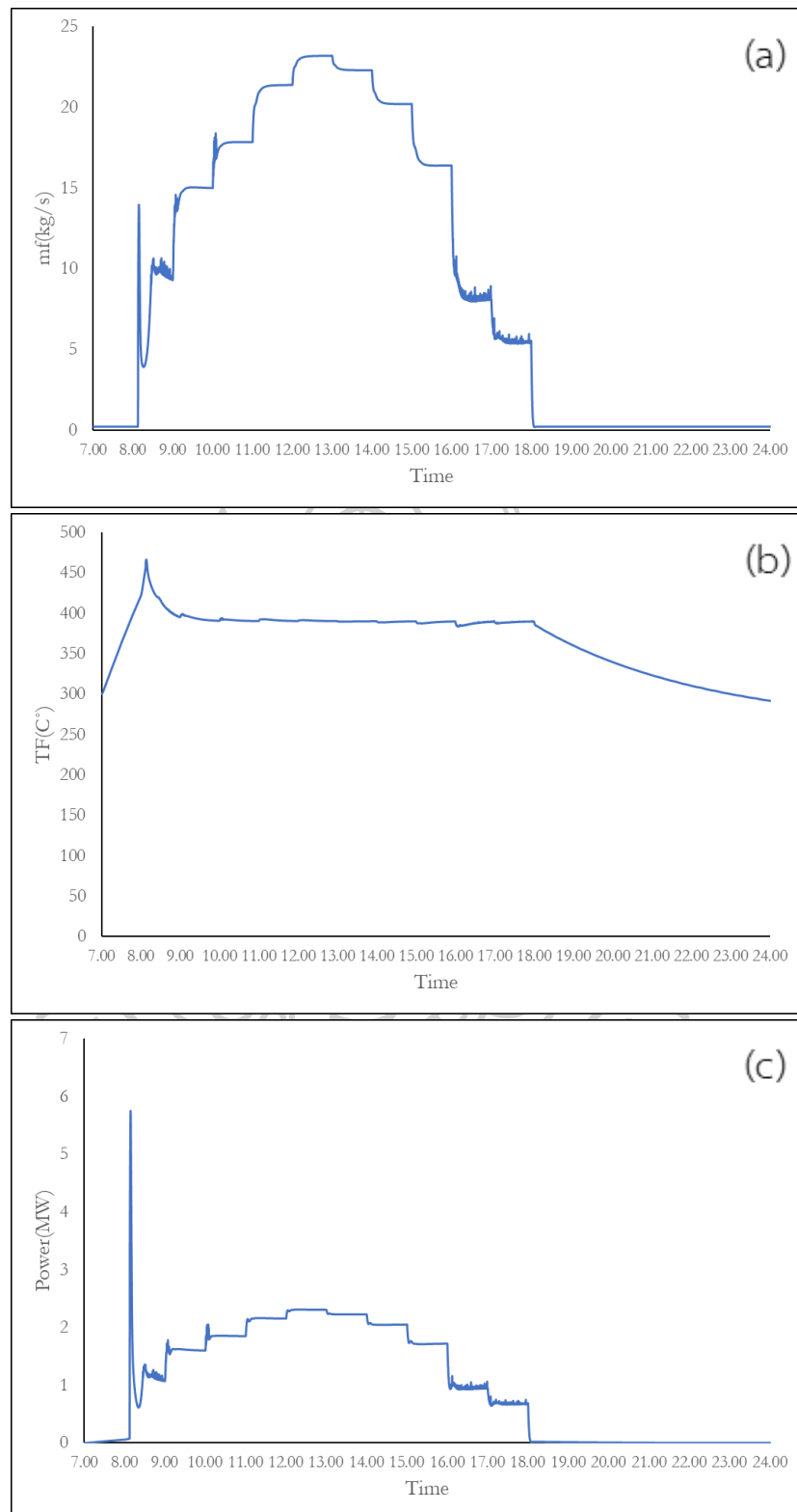
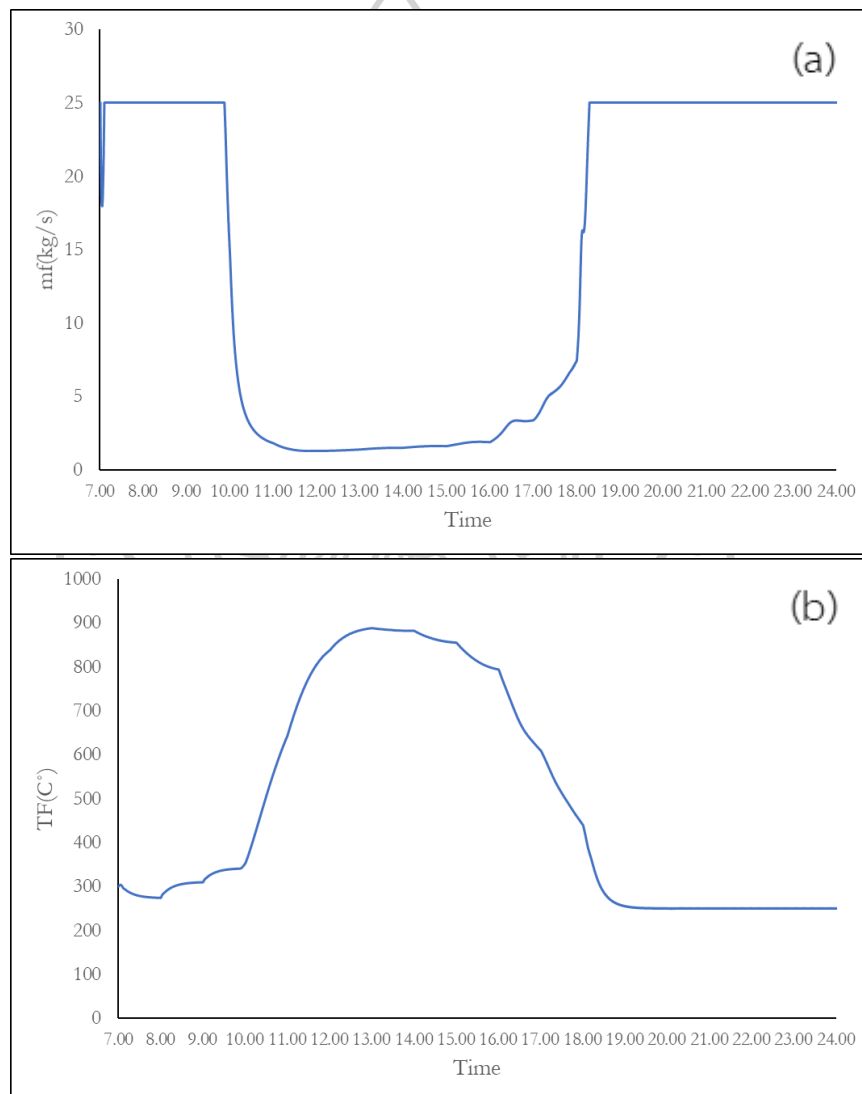


Figure 21 Closed-loop response of temperature control configuration: (a) the flow rate of HTF, (b) the outlet temperature of the collector, and (c) the power generation of the solar thermal power plant.



### 5.2.2 Single loop control with power control configuration using continuous-time PI.

In power control configuration, the PI control system was designed to keep the power generation at 1 MW. The closed-loop response of the power control configuration is shown in Figure 22. Figure 22c showed the power could reach 1 MW after the time 10.00 and stay there during a day until 10.00 where the sunlight was almost over, the power dropped below the target.



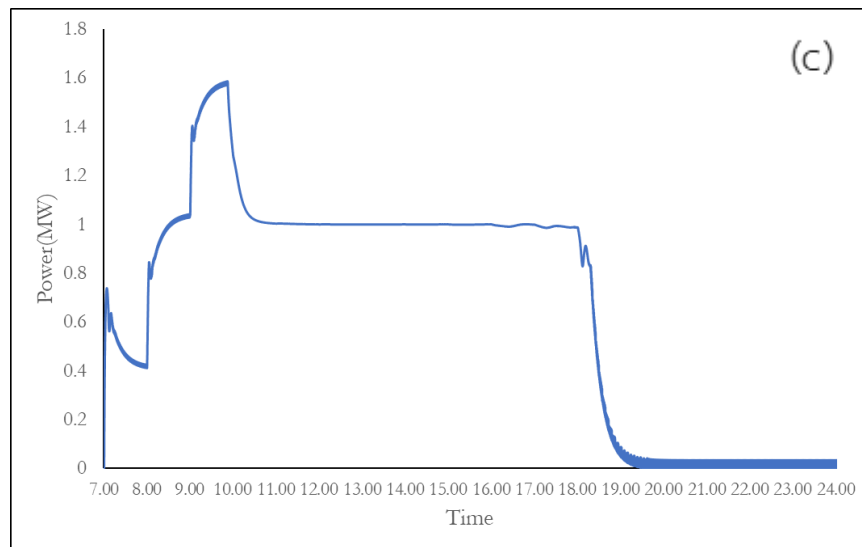


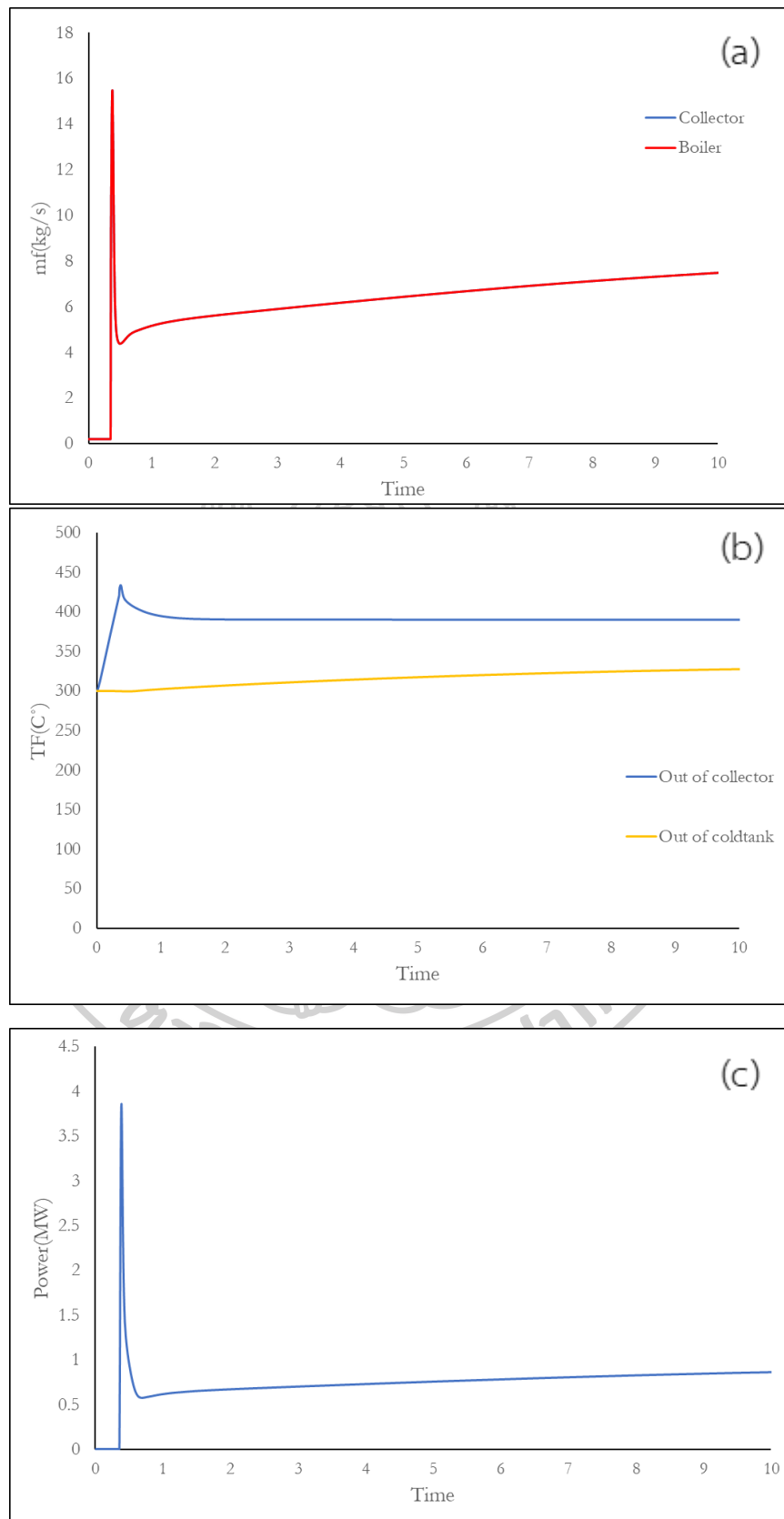
Figure 22 Closed-loop response of power control configuration: (a) the flow rate of HTF, (b) the outlet temperature of the collector, and (c) the power generation of the solar thermal power plant.

### 5.2.3 Dual-loop control using continuous-time PI

In this section, the simulation was firstly studied for the simple cases of constant solar irradiation at 450 and 800 W/m<sup>2</sup>. After that simulation for the case of varied solar irradiation during a day was studied.

For solar irradiation=450 W/m<sup>2</sup>, the control system was designed to keep the collector outlet temperature at 390 °C by manipulating the flow rate of the HTF input collector (charging loop) and keep the power generation at 1 MW by manipulating the flow rate of HTF out of the hot tank (discharging loop). The Dual loop control response was shown in Figure 23.

From Figure 23b, the HTF outlet temperature could reach the setpoint with an overshoot as the spike of the HTF flow rate of the collector (charging loop) in Figure 23a. For power control, the power could not be kept at the desired setpoint as the HTF flow rate of the boiler (discharging loop) had to adjust to the same value of the flow rate in the charging loop following the logic of the tanks to prevent overflow and underflow as shown in Figure 23d.



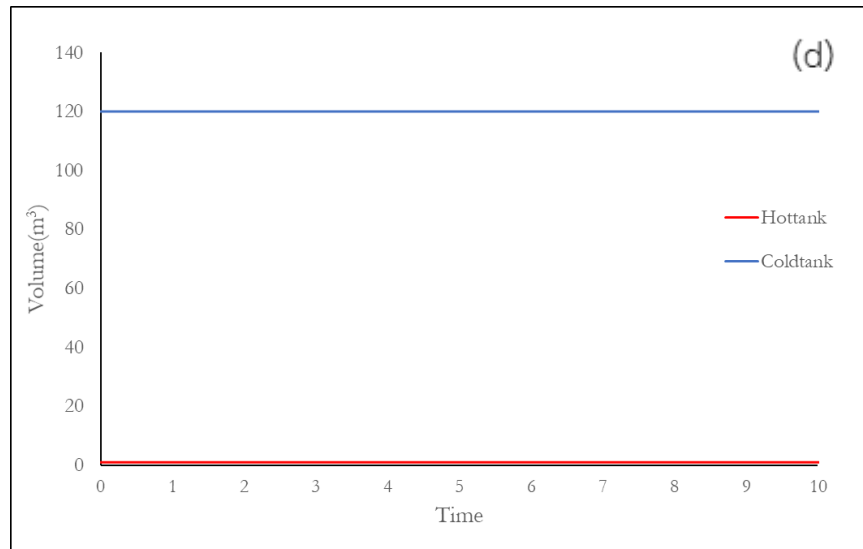
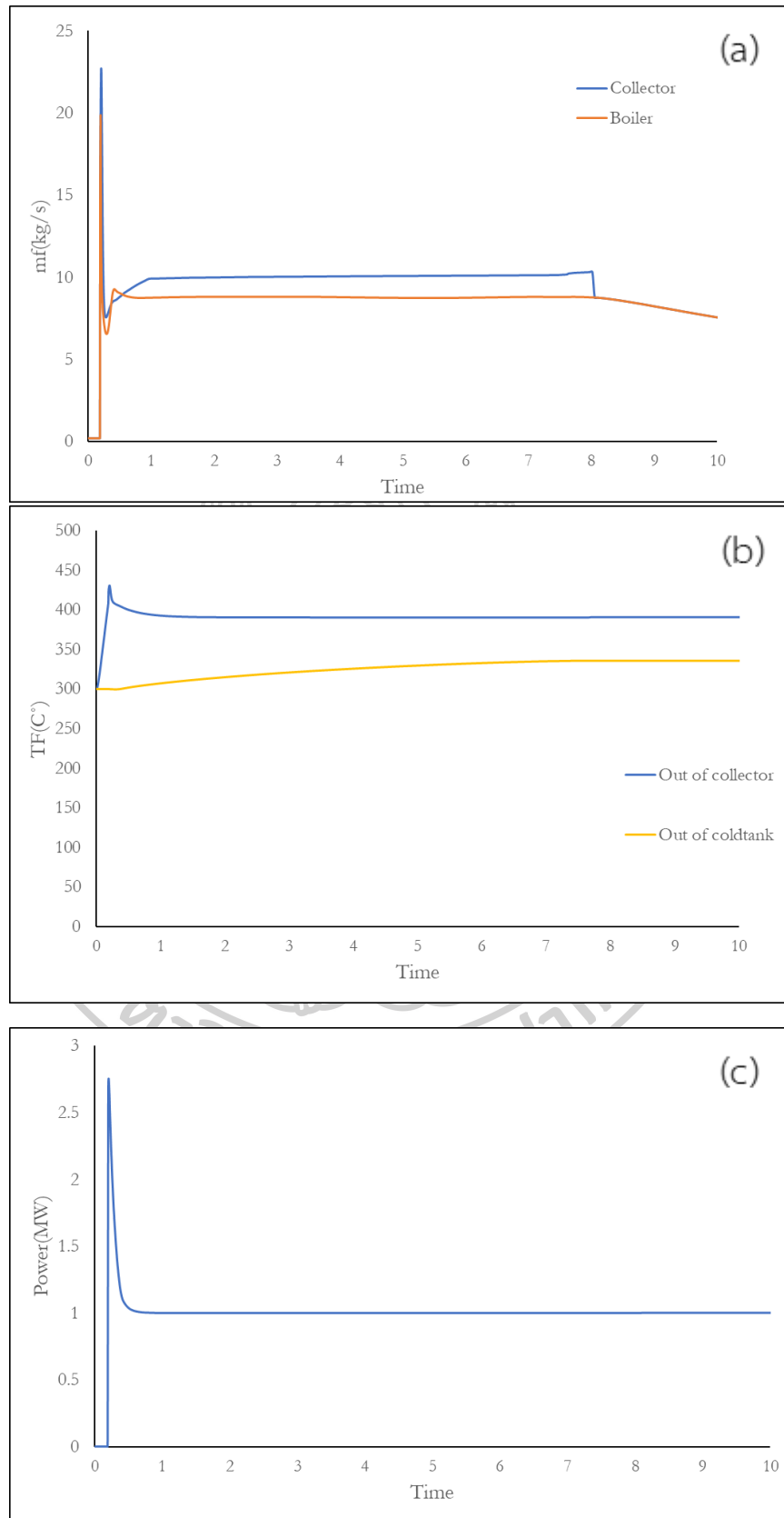


Figure 23 Closed-loop response of dual-loop PI control (a) The flow rate of HTF for collectors and cold tank in solar thermal power plants (b) Temperatures for solar thermal power plants (c) Power generation for solar thermal power plants (d) Volume of solar thermal storage tank for solar thermal power plants with solar irradiation is  $450 \text{ W/m}^2$ .

Figure 24 showed the result of the simulation of a solar thermal power plant operated at solar irradiation is  $800 \text{ W/m}^2$ . It could be found that the temperature could reach the target at  $390 \text{ }^\circ\text{C}$  as shown in Figure 24b. For power generation, the power could be kept at 1 MW. There were no overflow and underflow problems on the tanks until time = 8 as shown in Figure 24d where the HTF flow rate of discharging line was switched. However, after time = 8 the power could still be kept around the setpoint. This might be because the larger the HTF flow rate, the smaller the effect of the flow rate on the power as previously shown in Figure 24c.



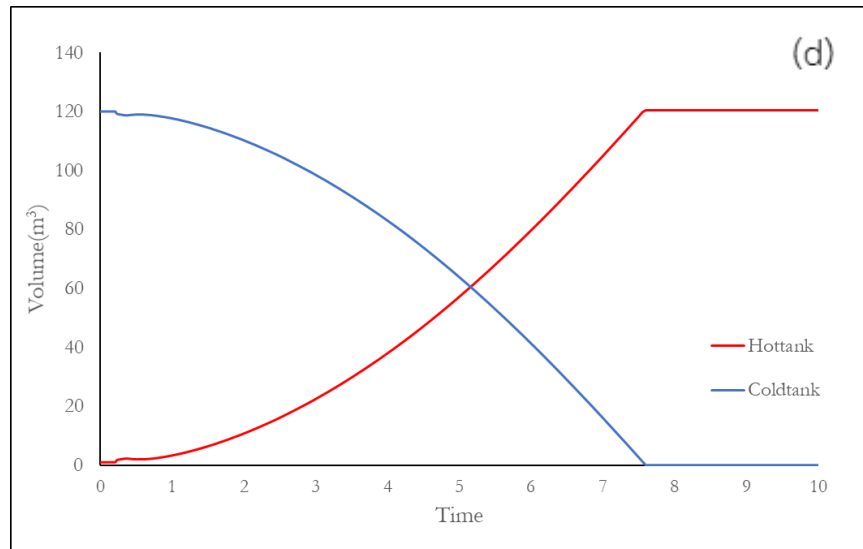
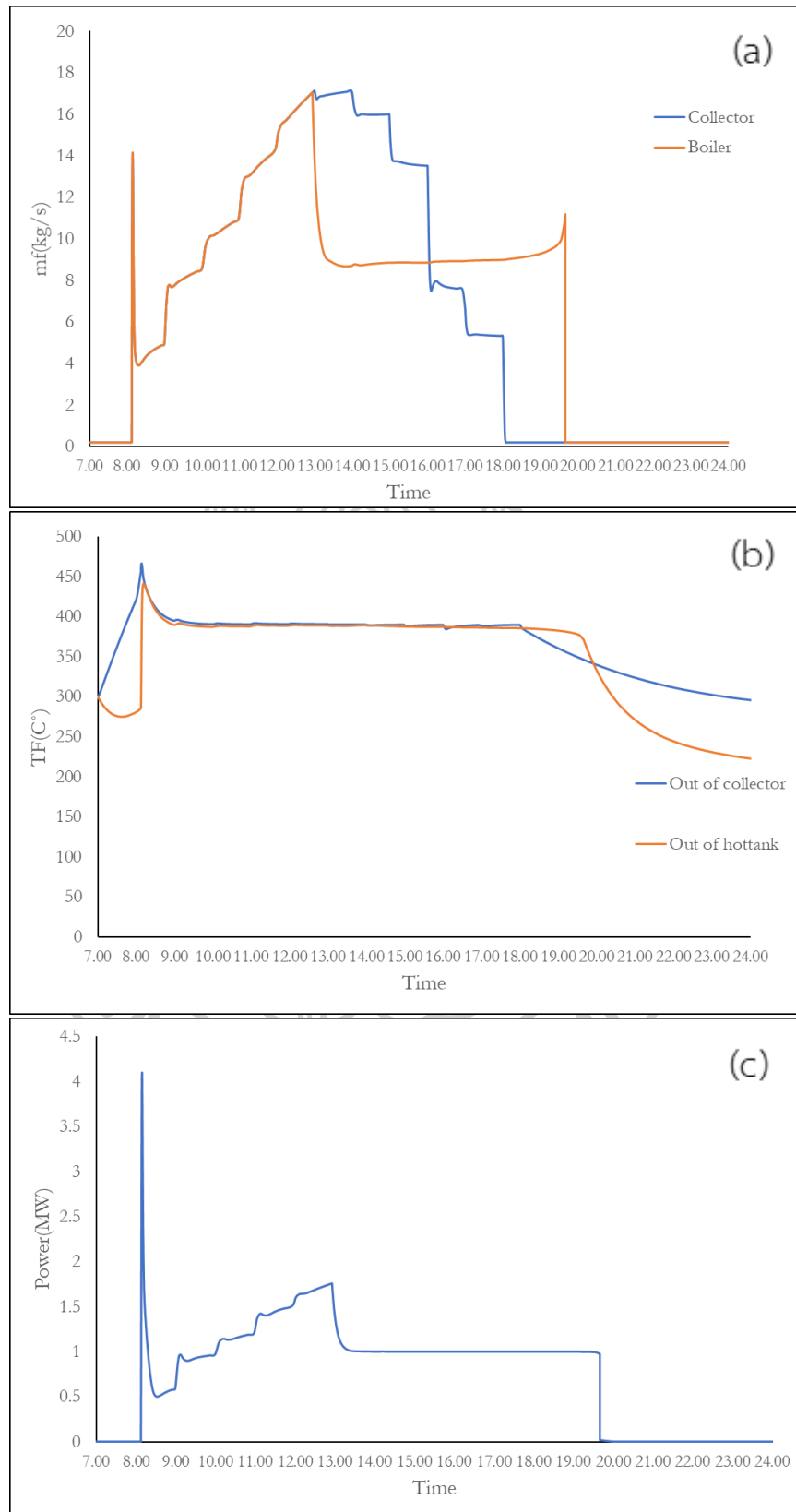


Figure 24 Closed-loop response of dual-loop PI control (a) The flow rate of HTF for collectors and cold tank in solar thermal power plants (b) Temperatures for solar thermal power plants (c) Power generation for solar thermal power plants (d) Volume of solar thermal storage tank for solar thermal power plants with solar irradiation is  $800 \text{ W/m}^2$ .

Previous studies were based on constant solar irradiation. For a more realistic case, varied solar irradiation during a day was further studied here. As shown in Figure 25b, the HTF outlet temperature could be kept at the setpoint with some overshoot since 09.00 am while the power needs almost half a day to be kept at the setpoint as shown in Figure 25c. This was due to overflow/underflow problems on the tanks during 07.00-13.00 as shown in Figure 25d resulting in the switching of the flow rate in Figure 25a. Furthermore, after 18.00, the HTF temperature dropped below the setpoint due to the finish of sunlight. However, the power could still be kept further for a while until 20.00 where the heat of the hot tank was over.



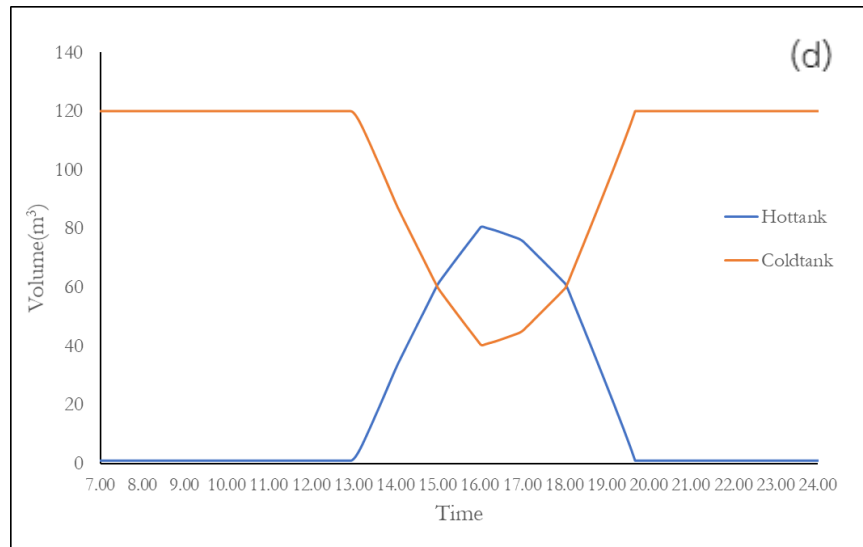


Figure 25 Closed-loop response of dual-loop PI control (a) The flow rate of HTF for collectors and Boilers in solar thermal power plants (b) Temperatures for solar thermal power plants (c) Power generation for solar thermal power plants (d) Volume of solar thermal storage tank for solar thermal power plants with solar irradiation on the time of day.

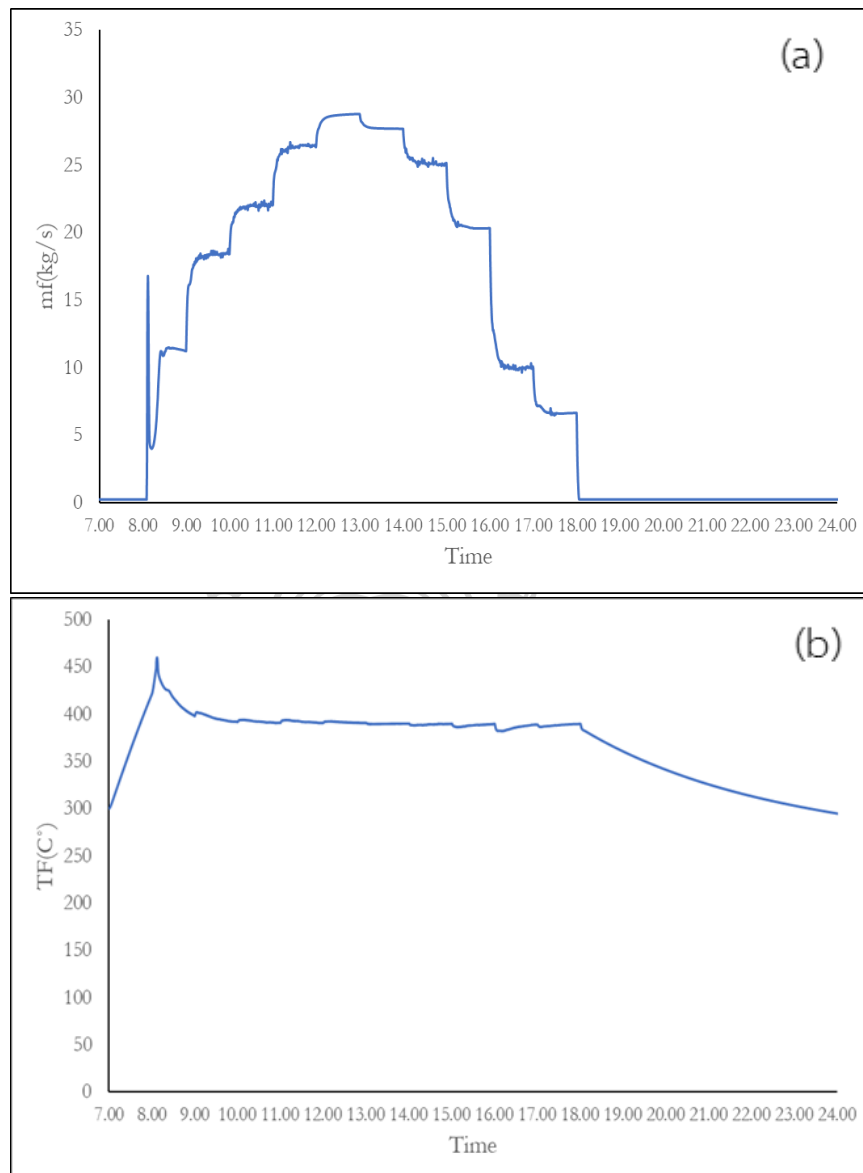
### 5.3 Closed-loop simulation with discrete-time PI

To be more realistic and to compare the performance with MPC which was discrete in nature, closed-loop control using discrete-time PI was studied. The sample time used was 0.1 hr.

#### 5.3.1 Single-loop control with temperature control configuration using discrete-time PI

In temperature control configuration, the discrete PI control system was designed to keep the collector outlet temperature at 390 °C. For a varied irradiation during a day, the temperature could be kept at the setpoint as shown in Figure 26b but with a variation of power generation as shown in Figure 26c.





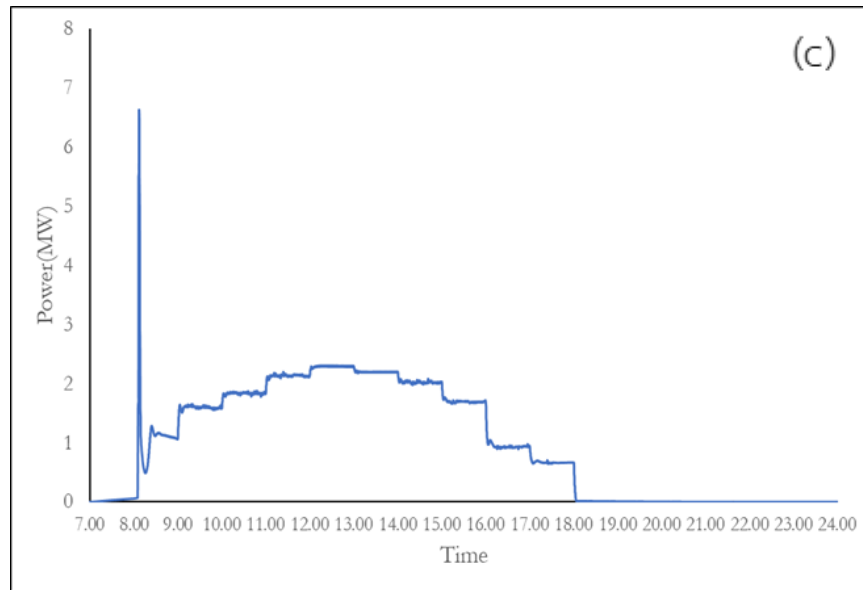
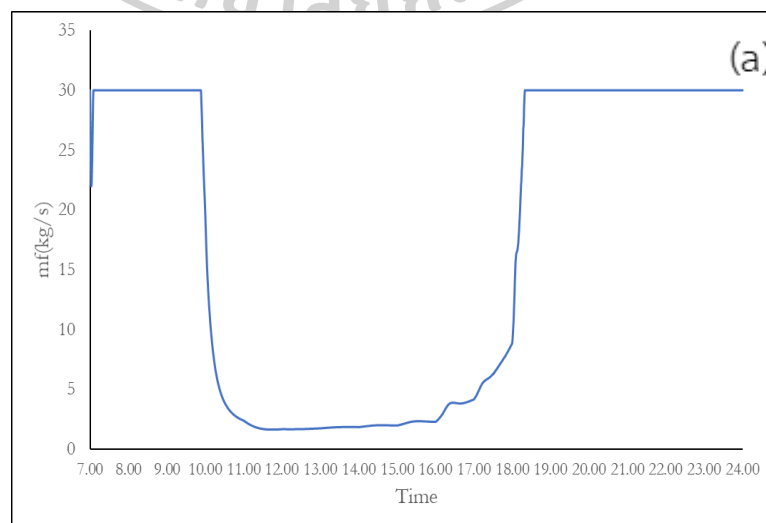


Figure 26 Closed-loop response of temperature control configuration with discrete-time PI : (a) the flow rate of HTF, (b) the outlet temperature of the collector, and (c) the power generation of the power plant.

### 5.3.2 Single-loop control with power control configuration using discrete-time PI

In temperature configuration, the PI control system was designed to keep the power generation at 1 MW. For a varied irradiation during a day, after some time the power could be kept at the setpoint as shown in Figure 27c but with a variation of the HTF temperature as shown in Figure 27b.



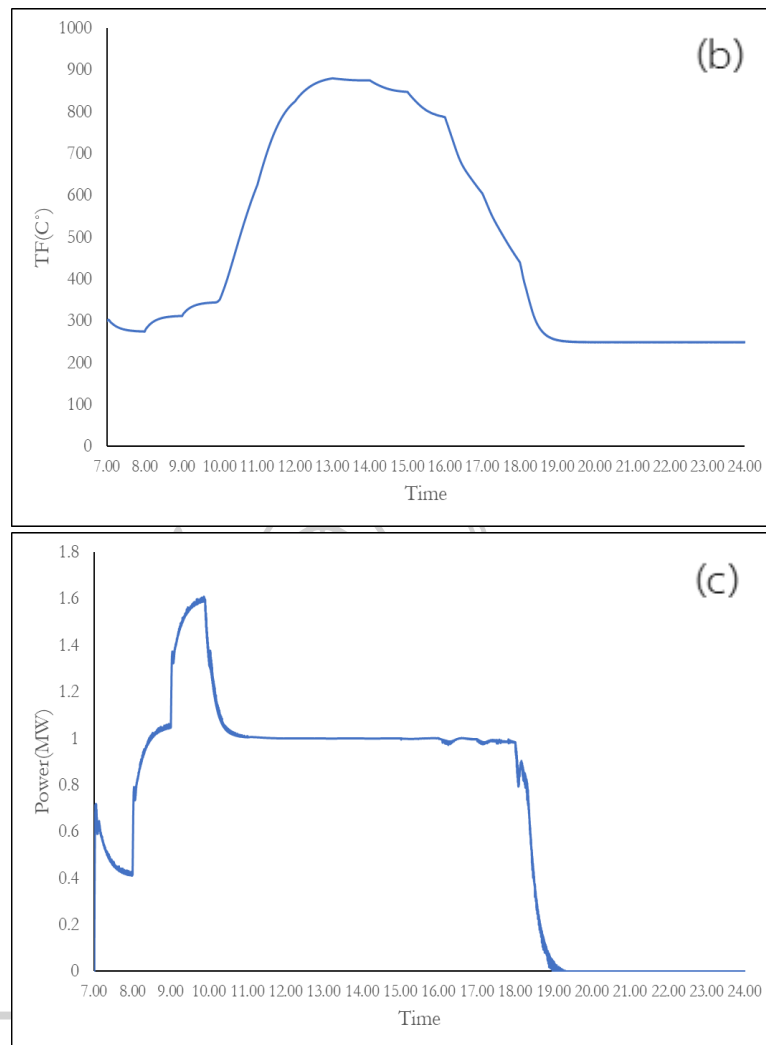


Figure 27 Closed-loop response of power control configuration with discrete-time PI: (a) the flow rate of HTF, (b) the outlet temperature of the collector, and (c) the power generation of the power plant.

### 5.3.3 Dual-loop control using discrete-time PI controllers

For dual-loop control using discrete-time PI, in our attempt, the plant could not be controlled for both the outlet HTF temperature and the power generation.

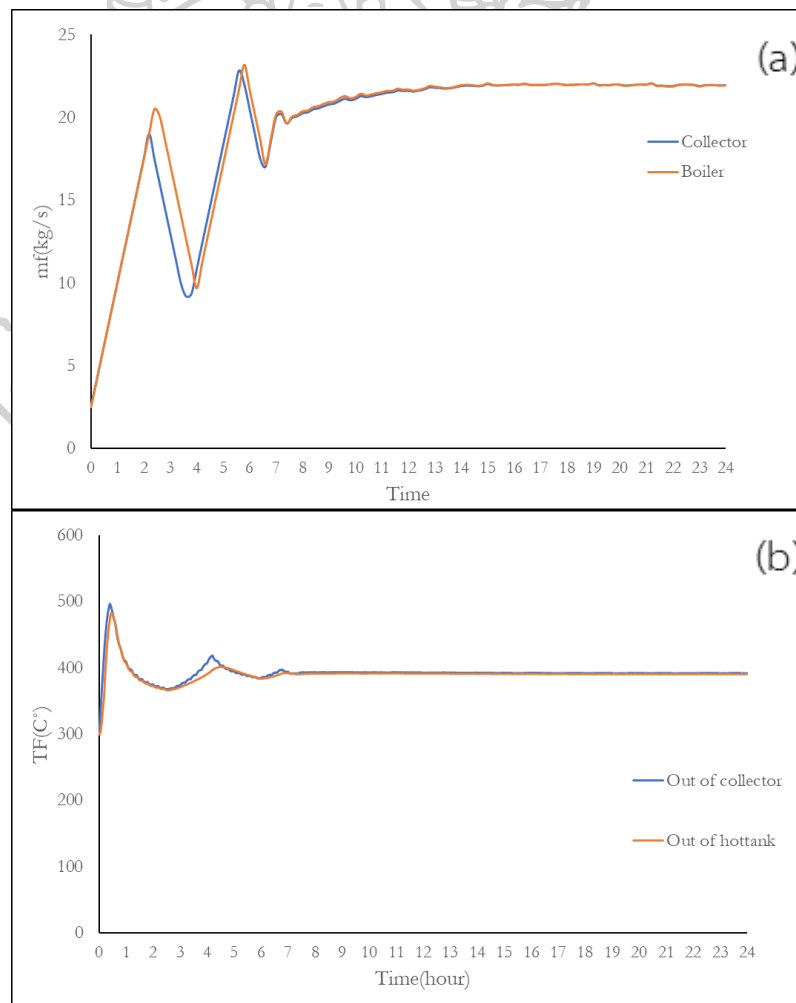
### 5.4 Closed-loop simulation with MPC control

In our attempt to control the power plant using MPC, dual-loop control could be achieved. Furthermore, for a varied irradiation, MPC could not provide satisfied

control results. Hence, here only the simulation with constant irradiation at  $800 \text{ W/m}^2$  was shown.

#### 5.4.1 Single-loop control with temperature control configuration using MPC

The process operated at the solar irradiation of  $800 \text{ W/m}^2$  and the target of the HTF outlet temperature collector was at  $390 \text{ }^\circ\text{C}$ . In MPC, two manipulated variables were used for control. The parameter used in MPC included sample time  $0.1 \text{ hr.}$ , the prediction horizon 25, and the control horizon 2. The result of the simulation was shown in Figure 28. Figure 28b showed the HTF outlet temperature could reach the target with some overshoots. The power generation was varied and reached  $1.8 \text{ MW}$  as shown in Figure 28c.



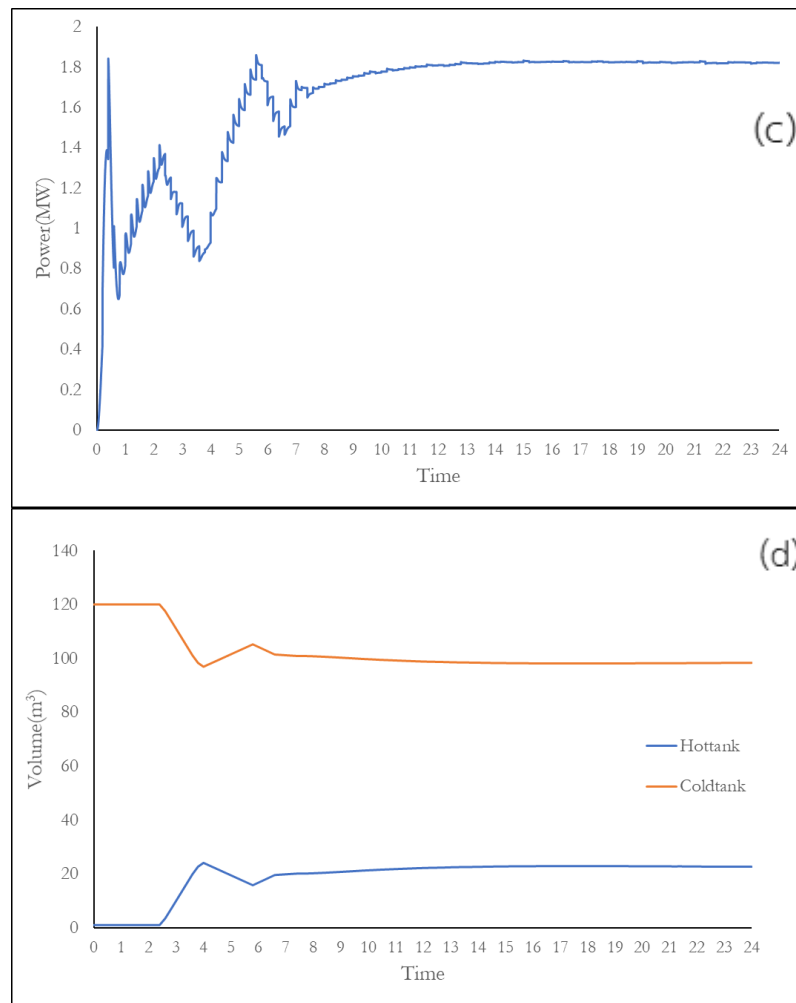
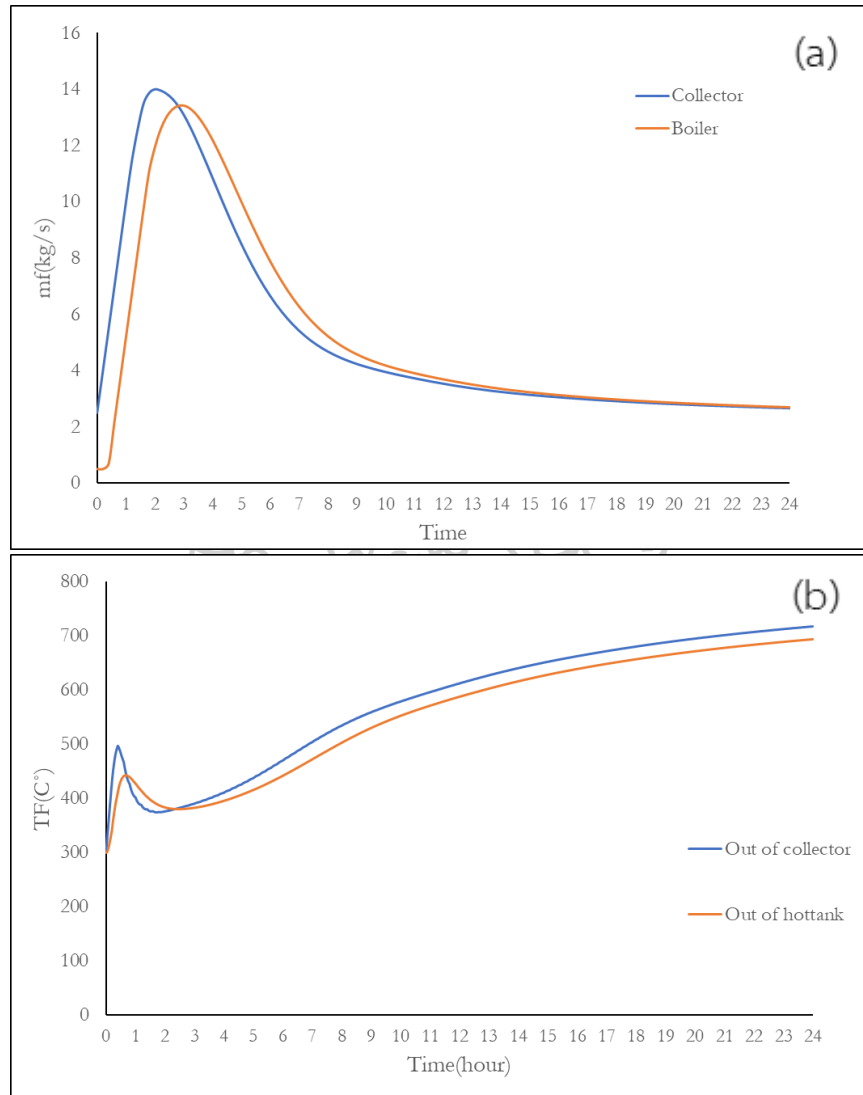


Figure 28 Closed-loop response of temperature control with MPC controller (a) The flow rate of HTF for collectors and Boilers in solar thermal power plants (b) Temperatures for solar thermal power plants (c) Power generation for solar thermal power plants (d) Volume of solar thermal storage tank for solar thermal power plants with solar irradiation is  $800 \text{ W/m}^2$ .

#### 5.4.2 Single-loop control with power control configuration using MPC

The process operated at the solar irradiation  $800 \text{ W/m}^2$  and the target of power generation at 1 MW. In MPC, two manipulated variables were used for control of the process. The MPC parameter included sample time 0.1 hr., the prediction horizon 25, and the control horizon 2. The result of the simulation was

shown in Figure 29. Figure 29c showed the power generation could reach the target while the temperature was not controlled.



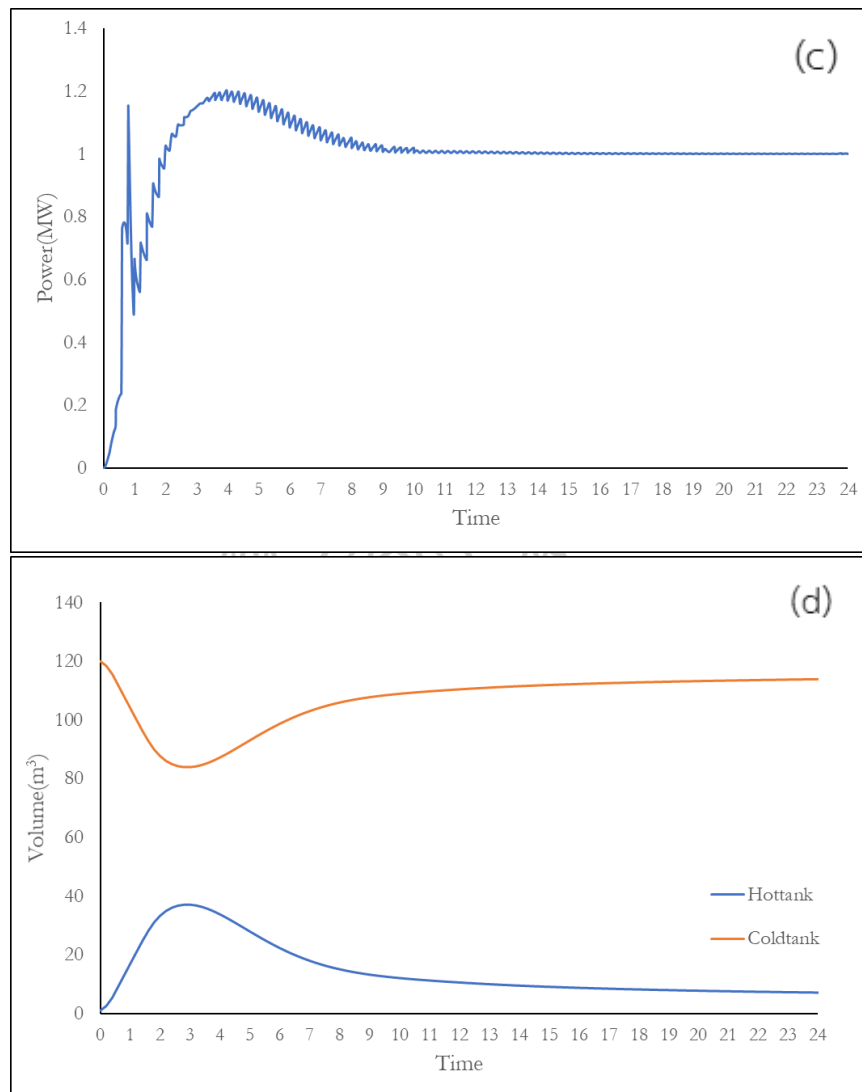
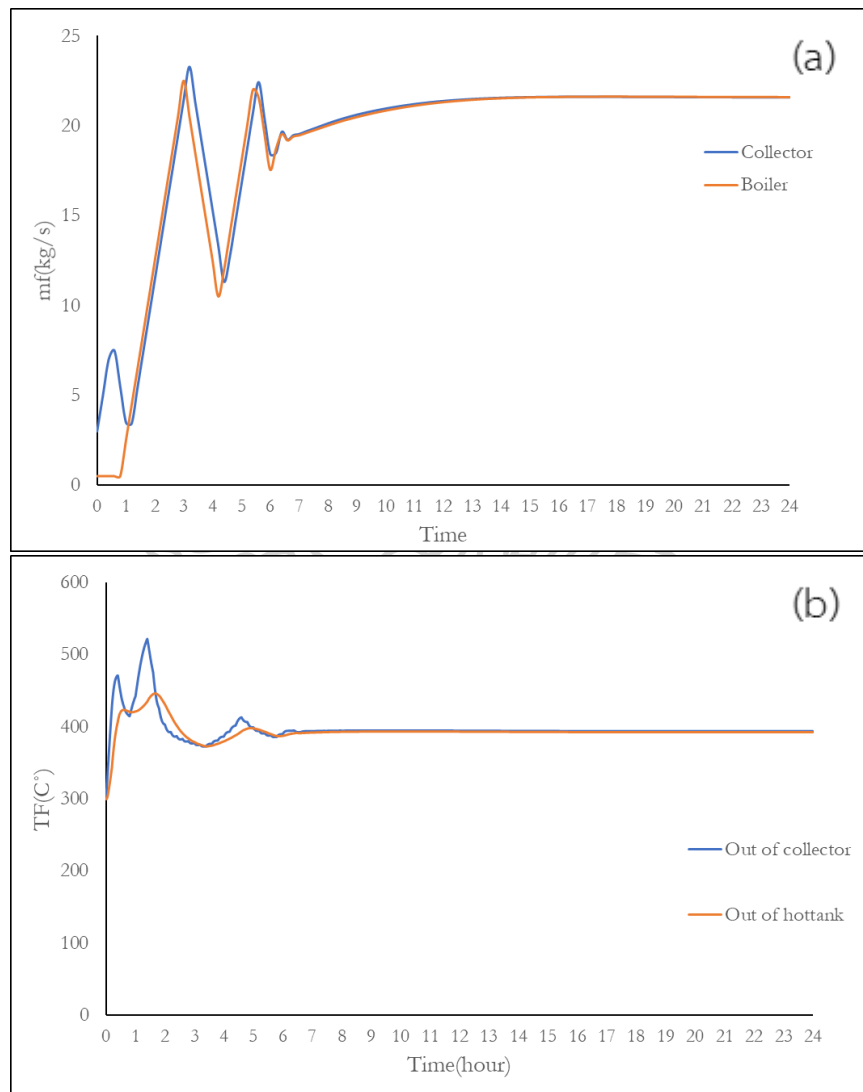


Figure 29 Closed-loop response of power control with MPC controller (a) The flow rate of HTF for collectors and Boilers in solar thermal power plants (b) Temperatures for solar thermal power plants (c) Power generation for solar thermal power plants (d) Volume of solar thermal storage tank for solar thermal power plants with solar irradiation is  $800 \text{ W/m}^2$ .

#### 5.4.3 Dual-loop control using MPC control

In dual-loop control, MPC was designed to keep the HTF outlet temperature at  $390 \text{ }^\circ\text{C}$  and the power generation at 1 MW by manipulating the flow rate of HTF passing the collector (charging loop) and the flow rate of HTF passing the boiler (discharging loop). The MPC tuning included sample time 0.1 hr., the prediction

horizon 25, and the control horizon 2. Simulation results showed that the temperature could be kept at the setpoint while the power could not be controlled as shown in Figure 30. Some attempts including adjusting weight in the objective function, prediction horizon, control horizon had been made but the control performance could not be achieved.





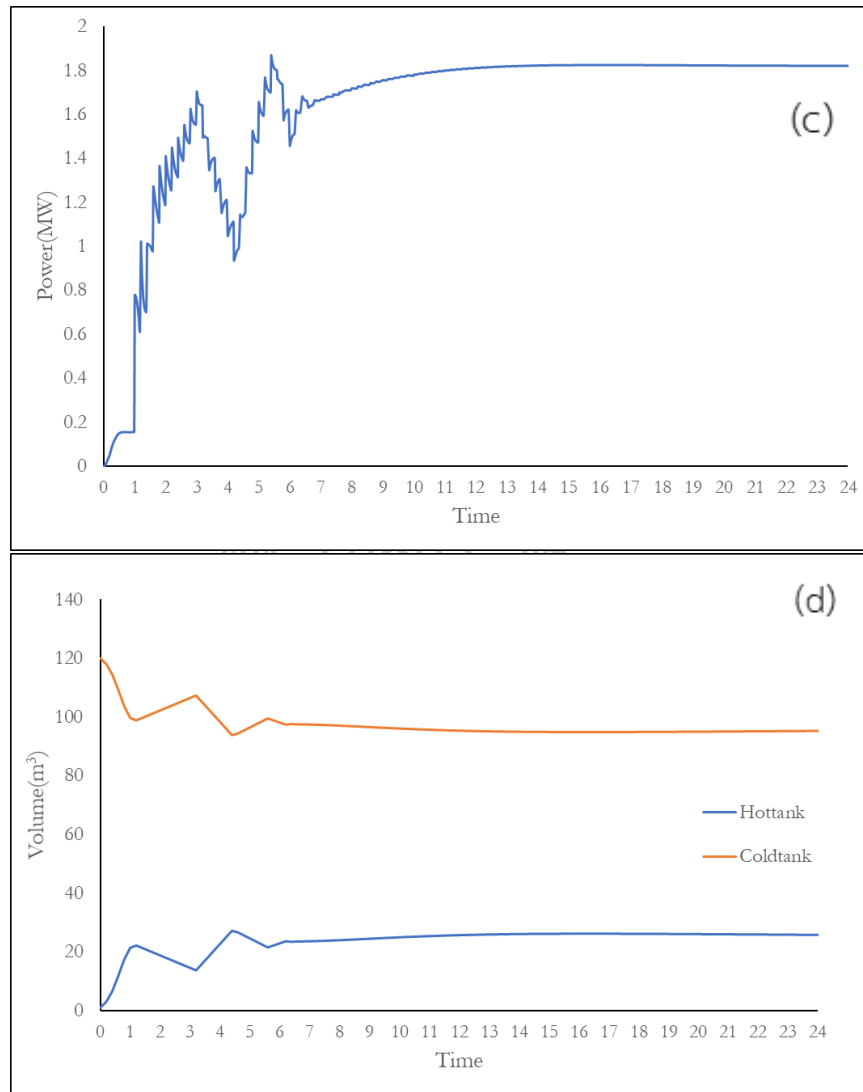


Figure 30 Closed-loop response of dual-loop control with MPC controller (a) The flow rate of HTF for collectors and Boilers in solar thermal power plants (b) Temperatures for solar thermal power plants (c) Power generation for solar thermal power plants (d) Volume of solar thermal storage tank for solar thermal power plants with solar irradiation is  $800 \text{ W/m}^2$ .

## CHAPTER VI

### CONCLUSION

The demand for energy consumption continuously increases while the availability of fossil energy steadily decreased. Solar energy is one of the main renewable options for power generation. However, unlike other sources of energy that can be manipulated, solar radiation acts as a disturbance that is uncertain and changes seasonal and on a daily base. Hence, control of solar thermal power plants is a challenging task. In this research, dynamic simulations of parabolic trough concentrated solar thermal power plants were performed in both open-loop and closed-loop to investigate the dynamic behavior of the power plant. The process and model used in this paper were adapted from Powell and Edgar.

In the open-loop simulation, effects of the flow rate of heat transfer fluid (HTF) to the outlet temperature of the collector and power generation under daily solar radiation were demonstrated. The results showed inherent nonlinearity in the power plant.

In the closed-loop simulation, three control configurations including single-loop HTF temperature control, single-loop power control, and dual-loop control (where both HTF temperature and power were controlled) were proposed. PI and MPC controllers were designed for each control configuration. In a closed-loop simulation using PI controller, continuous- and discrete-time PI were implemented. Continuous-time PI was implemented to see the possibility for control of the power plant in the ideal case while discrete-time PI was implemented for the comparison with MPC which was discrete in nature and more realistic. The results showed that continuous-time PI could keep all controlled variables at the setpoint for all control configurations while discrete-time PI and MPC could keep controlled variables at the setpoint for only some cases.

This work attempted to design MPC controller for control of the solar power plant. However, the attempt was not successful. This might be because the plant

was nonlinear while linear MPC was used. Further study on the implementation of nonlinear MPC for control of the power plant should be investigated.



## APPENDIX A

### PID tuning parameter

The process is highly nonlinear, it can't transform to transfer function with linearization. The method used to approximate First Order Plus Dead Time (FOPDT) Dynamics with Graphical fitting. It uses an open-loop simulation that allows the flow rate to change from 10 kg/s to 12 kg/s at solar irradiation (IC) equal 600 W/m<sup>2</sup> and sees how the system behavior changes.

#### 1 PI controller of temperature loop control

Figure 31 shows the result of the temperature outlet of the collector when step change of the flow rate out of the collector 10 kg/s to 12 kg/s. it finds the values of  $K_p$ ,  $\tau$ , and  $\theta$  following in the step.

- Find  $\Delta x$  and  $\Delta y$  from step response
- Calculate  $K_p = \frac{\Delta y}{\Delta x} = \frac{392.0029695 - 398.6537524}{12 - 10} = -3.325391462$
- Find  $\theta = (1.3t_{35.3\%} - 0.29t_{83.5\%})$   
 $= (1.3 \times 10.02469766) - (0.29 \times 10.06523704)$   
 $= 10.11318822$
- Calculate  $\tau = 0.67(t_{35.3\%} - t_{83.5\%})$   
 $= 0.67(10.06523704 - 10.02469766)$   
 $= 0.027161383$

$$K_p = -3.325391462, \tau = 0.027161383, \theta = 10.11318822$$

Input  $K_p$ ,  $\tau$ , and  $\theta$  to model Consider the standard FOPTD model.

$$\tilde{G}(s) = \frac{K_p e^{-\theta s}}{\tau s + 1} = \frac{-3.325391462 e^{-10.11318822s}}{0.027161383s + 1}$$

From Table 1 IMC-Based PID Controller Settings for  $G_c(s)$ , the given process model is similar to controllers G to get PI parameter. We can calculate  $K_c$  and  $\tau_i$  if

$\tau_c = 0.2$  follow in the equation.

$$K_c = \frac{1}{K_p} \frac{\tau}{\theta + \tau_c} = \frac{1}{-3.325391462} \left( \frac{0.027161383}{10.11318822 + 0.2} \right) = -0.000791984$$

$$\tau_i = \tau = 0.027161383$$

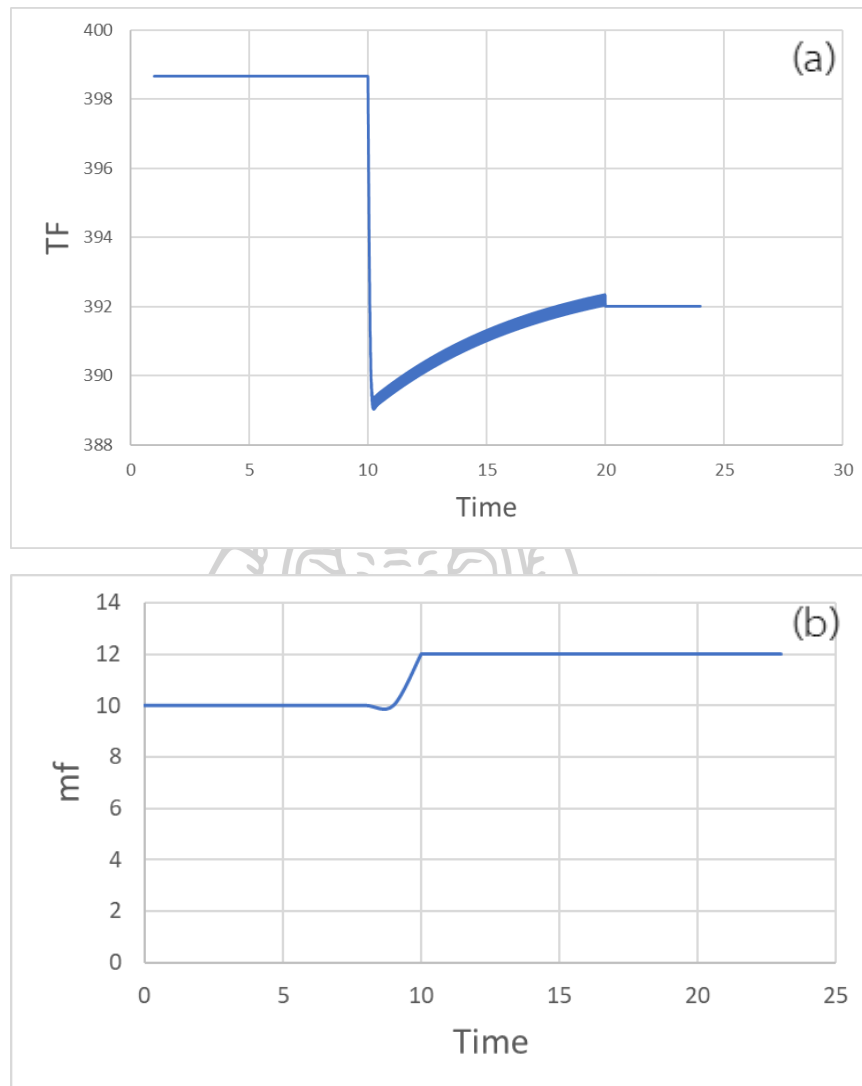


Figure 31 (a) the simulation between the temperature outlet of the collector when the flow rate of HTF changes, (b) the flow rate of HTF changes from 10 kg/s to 12 kg/s at IC = 600 W/m<sup>2</sup>.

### 2 PI controller of temperature loop control

Figure 32 shows the result of the power generation when step change of the flow rate out of the collector 10 kg/s to 12 kg/s. it finds the values of  $K_p$ ,  $\tau$ , and  $\theta$  following in the step.

- Find  $\Delta x$  and  $\Delta y$  from step response

- Calculate  $K_p = \frac{\Delta y}{\Delta x} = \frac{1.313201358 - 1.178006841}{12 - 10} = 0.067597258$
- Find  $\theta = (1.3t_{35.3\%} - 0.29t_{83.5\%})$   
 $= (1.3 \times 10.09661274) - (0.29 \times 15.38394737)$   
 $= 8.664251826$
- Calculate  $\tau = 0.67(t_{35.3\%} - t_{83.5\%})$   
 $= 0.67(15.38394737 - 10.09661274)$   
 $= 3.542514203$

$$K_p = 0.067597258, \tau = 3.542514203, \theta = 8.664251826$$

Input  $K_p$ ,  $\tau$ , and  $\theta$  to model. Consider the standard FOPTD model.

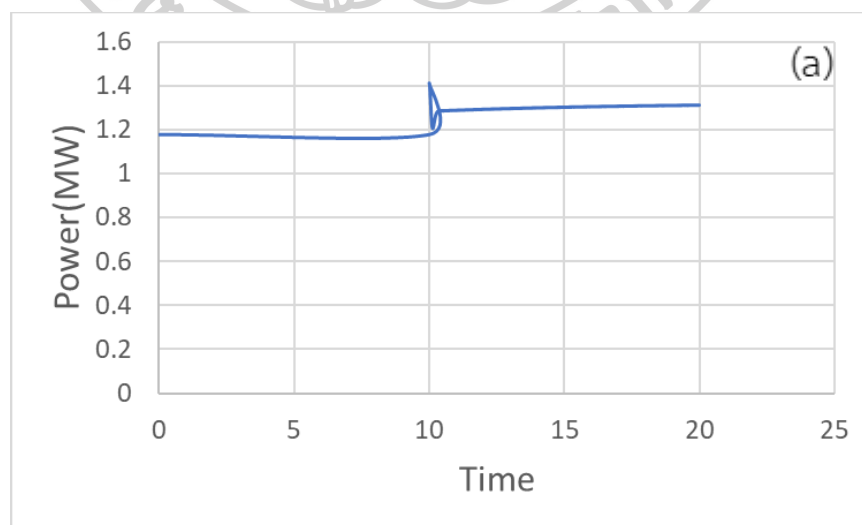
$$\tilde{G}(s) = \frac{K_p e^{-\theta s}}{\tau s + 1} = \frac{0.067597258 e^{-8.664251826s}}{3.542514203s + 1}$$

From Table 1 IMC-Based PID Controller Settings for  $G_c(s)$ , the given process model is similar to controllers  $G$  to get PI parameter. We can calculate  $K_c$  and  $\tau_i$  if

$\tau_c = 0.2$  follow in the equation.

$$K_c = \frac{1}{K_p} \frac{\tau}{\theta + \tau_c} = \frac{1}{0.067597258} \left( \frac{3.542514203}{8.664251826 + 0.2} \right) = 5.912081774$$

$$\tau_i = \tau = 3.542514203$$



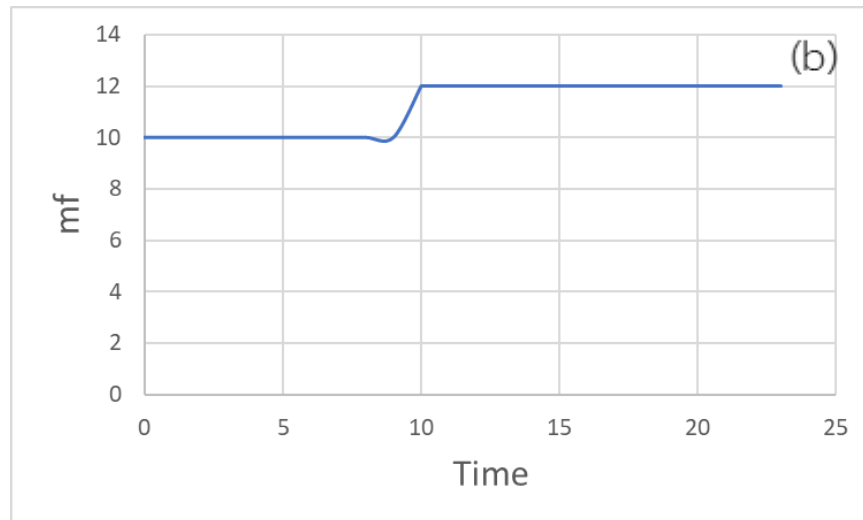
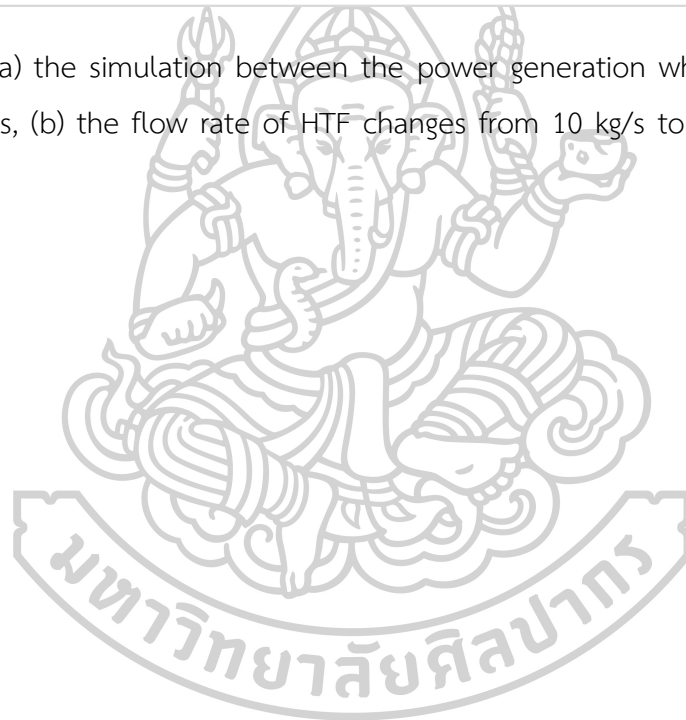


Figure 32 (a) the simulation between the power generation when the flow rate of HTF changes, (b) the flow rate of HTF changes from 10 kg/s to 12 kg/s at IC = 600 W/m<sup>2</sup>.



## REFERENCES

1. Outlook, A.E.J.D.o.E., *Energy information administration*. 2010. **92010**(9): p. 1-15.
2. Monica, O. *Renewable energy types*. 2017; Available from: [https://www.123rf.com/photo\\_53823512\\_stock-vector-renewable-energy-types-power-plant-icons-set-renewable-alternative-solar-wind-hydro-biofuel-geotherm.html](https://www.123rf.com/photo_53823512_stock-vector-renewable-energy-types-power-plant-icons-set-renewable-alternative-solar-wind-hydro-biofuel-geotherm.html).
3. Price, H., et al., *Advances in parabolic trough solar power technology*. 2002. **124**(2): p. 109-125.
4. Quaschnig, V.J.R.E.W., *Technology fundamentals-solar thermal power plants*. 2003. **6**(1): p. 09-113.
5. Powell, K.M. and T.F.J.C.E.S. Edgar, *Modeling and control of a solar thermal power plant with thermal energy storage*. 2012. **71**: p. 138-145.
6. Forristall, R., *Heat transfer analysis and modeling of a parabolic trough solar receiver implemented in engineering equation solver*. 2003, National Renewable Energy Lab., Golden, CO.(US).
7. Conrado, L.S., et al., *Thermal performance of parabolic trough solar collectors*. 2017. **67**: p. 1345-1359.
8. Yilmaz, İ.H. and A.J.A.e. Mwesigye, *Modeling, simulation and performance analysis of parabolic trough solar collectors: A comprehensive review*. 2018. **225**: p. 135-174.
9. Fan, M., et al., *Applicability analysis of the solar heating system with parabolic trough solar collectors in different regions of China*. 2018. **221**: p. 100-111.
10. Padilla, R.V., et al., *Heat transfer analysis of parabolic trough solar receiver*. 2011. **88**(12): p. 5097-5110.
11. Seborg, D.E., et al., *Process dynamics and control*. 2010: John Wiley & Sons.
12. Levine, W.S., et al., *Handbook of model predictive control*. 2018.
13. Bergman, T.L., et al., *Fundamentals of heat and mass transfer*. 2011. 2015, John Wiley & Sons.
14. Aekapan Padsri, K.K., and Akarin Intaniwet, *Efficiency and Performance Analysis*



*of a 300 kW Grid-tied Solar Power Generation System. The 3rd KU SRC Annual Conference, 2018: p. 95-104.*





## VITA

**NAME** Chanachai Mahom

**DATE OF BIRTH** 7 May 1993

**PLACE OF BIRTH** Siriraj hospital Bangkok

**INSTITUTIONS ATTENDED** Department of Chemical Engineering Silpakorn University

**HOME ADDRESS** 251 Moo 4, Phok Noi Subdistrict, Phanna Nikhom District  
Sakon Nakorn 47220

